# Using Valence Bond Theory to Understand Electronic Excited States: Application to the Hidden Excited State (21Ag) of C2nH2n+2(n= 2−14) Polyenes

**ARTICLE** *in* THE JOURNAL OF PHYSICAL CHEMISTRY A · SEPTEMBER 2000

Impact Factor: 2.69 · DOI: 10.1021/jp000847h



**4 AUTHORS:**

Wei Wu
Indiana University-Purdue University Indiana…
**82** PUBLICATIONS **1,174** CITATIONS
SEE PROFILE

David Danovich
Hebrew University of Jerusalem
**114** PUBLICATIONS **2,352** CITATIONS
SEE PROFILE

A. Shurki
Hebrew University of Jerusalem
**49** PUBLICATIONS **1,308** CITATIONS
SEE PROFILE

Sason Shaik
Hebrew University of Jerusalem
**527** PUBLICATIONS **20,695** CITATIONS
SEE PROFILE

# Using Valence Bond Theory to Understand Electronic Excited States: Application to the Hidden Excited State ($2^1A_g$) of $C_{2n}H_{2n+2}$ ($n = 2-14$) Polyenes

**Wei Wu,*,† David Danovich,‡ Avital Shurki,‡ and Sason Shaik*,‡**

*Department of Chemistry and State Key Laboratory for Physical Chemistry of the Solid Surface, Xiamen University, Xiamen, Fujian 361005, P. R. of China, and Department of Organic Chemistry and the Lise Meitner-Minerva Center for Computational Quantum Chemistry, The Hebrew University, Jerusalem 91904, Israel*

*Received: March 3, 2000; In Final Form: June 23, 2000*

A valence bond (VB) method is presented and applied to calculate the hidden excited states, $2^1A_g$, and other covalent excited states of polyenes from $C_4H_6$ to $C_{28}H_{30}$. The ground rules needed to understand the results are qualitatively outlined and used to discuss the asymptotic behavior of these molecules as *n* goes to infinity. The theory enables to understand in a coherent and lucid manner excited state properties, such as the makeup of the various states, their energies and geometries, the puzzling increase of the C═C frequency in the excited state, the opposite bond alternation properties of the ground and excited state, isomerization patterns, soliton characteristics, etc.

## I. Introduction

One of the most powerful approaches to conceptualize and predict chemical behavior is provided by valence bond (VB) theory.[1] A special area where the use of VB theoretic ideas may have a serious conceptual impact is the electronic structure and reactivity patterns of excited states.[2] In this paper we extend our recently developed VB method, scaled to density functional energies,[3] to compute the ground and covalent excited states of polyenes $C_{2n}H_{2n+2}$ (from $n = 2$ to $n = 14$), and in so doing we also develop tools and qualitative guides required to understand trends across the polyene series. Polyenes are versatile molecules with a great deal of appeal to the chemistry, biochemistry, and physics communities. In their ground or doped states, polyenes conduct electricity. While the doped states are metallic, the neutral ground states are semiconductors with a finite intrinsic gap. In their excited states, these molecules are important in several key processes in nature, such as vision and light harvesting.[4−7] It is no surprise therefore that this molecular family has become an arena for experimental and theoretical treatments.

One of the excited states which has attracted considerable attention is the "hidden" excited state, $2^1A_g$, which is dipole forbidden. Since the discovery of this state by Hudson and Kohler,[8,9] the "hidden" excited state has continued to occupy a central theme in polyene chemistry. The pioneering study of Karplus and Schulten[10] designed to understand the ordering of the $1^1 B_u^+ - 2^1A_g$ states has shown that the $2^1A_g$ state is formally a doubly excited one, whereas $1^1 B_u^+$ is a singly excited state, and that therefore the correct ordering of these states requires inclusion of doubly excited configurations in the configuration interaction treatment. After this study, and following two-photon excitation experiments, it was established that the $2^1A_g$ state is the first vertical excited state, for all polyenes starting with $C_8H_{10}$ onward,[4−7] and is likely to be the first adiabatic excited state even for shorter polyenes. The most sophisticated calculations to date, complete active space self-consistent field followed by second-order perturbation treatment (CASPT2)[11−13] and multireference Möller−Plessett perturbation (MRMP) calculations,[14,15] further establish this trend up to $C_{10}H_{12}$.

This hidden state exhibits a few interesting features which are summarized in excellent reviews.[4−7] For example, the $1^1A_g \rightarrow 2^1A_g$ excitation energy decreases steeply with *n* but converges to a finite value.[16−19] Both the ground[20−22] $1^1A_g$ and the excited[4−7,14] $2^1A_g$ states seem to sustain significant bond alternation, albeit in opposite manners. The totally symmetric C═C stretch mode in the hidden state has a frequency, $\omega_{C=C}(2^1A_g)$, which is considerably higher than the corresponding frequency of the ground state. This is reminiscent of the exalted $b_{2u}$ frequency in benzene, acenes, and in annulenes in the $1^1B_{2u}$ excited state.[23] Excited-state isomerization mechanisms of the mono-cis isomer to the all-trans and various other isomers is an active field of study[5] due to its potential association with isomerization that triggers the visual mechanism. Radiationless decay patterns depend on the size of the polyene in an irregular manner.[4,5] Add to that the question of solitons which are observed for these states[4,24] and their possible relation to the isomerization pathways, and one has at hand a fascinating multidimensional problem. Many of the features of these states have been addressed before with various methods and models, and there is a considerable degree of understanding of the problem in terms of ideas such as vibronic coupling[4−7,25] and modified Hückel treatment,[5,16] which start with the molecular orbital formulation of the states. Nevertheless, a VB method which combines simplicity and accuracy, and which enables understanding of the asymptotic behavior of these molecules as *n* goes to infinity, is still desirable and may add complementary insight to the existing models.

Already, in the pioneering work of Schulten and Karplus[10] it was noted that a VB formulation of the problem leads to a clear and simple understanding of both the ground and the hidden excited states of butadiene. The same insight was provided some time later by Simmoneta et al.,[26] and Hudson et al.,[4] Ohmine

† Xiamen University.
‡ The Hebrew University.

10.1021/jp000847h CCC: $19.00 
Published on Web 08/30/2000

et al.,[19] and Dunning and co-workers[27] have further shown that a fragments-in-molecules VB approach (excitonic model) is very useful for understanding the ordering pattern of the excited states in butadiene. Subsequently, Malrieu et al.[28] have developed an empirical VB model based on the Heisenberg Hamiltonian and scaled to ab inito energies and provided significant insight and understanding of the polyene states. More recent treatments of the ground state have been presented by Klein et al.[29] A very recent treatment of Li and Paldus[30] used the Hiesenberg Hamiltonian with Rumer VB structures to discuss the behavior of the $1^1B_u^-$ state and showed the potential of VB theory to present a coherent and simple picture which extends from the smallest member all the way to an infinite polyene. Hirao and collaborators[14,15,31] used a complete active space SCF to generate a CASVB wave function and to apply it to excited states of a few polyenes. Here we use our recently developed VBDFT(s) approach[3] which is a VB method scaled to density functional energies. The method was shown to reproduce ground-state properties very well.[3,32] In the present paper we show that VBDFT(s) which uses Rumer structures that are the canonical chemical structures, provides accurate excitation energies which are at par with sophisticated methods such as CASPT2[11,12] and MRMP,[14] for both $2^1A_g$ and $1^1B_u^-$ states. We develop a qualitative VB theory which enables to discuss the makeup of the various states, their energies and geometries, and other properties, such as the C=C frequency and bond alternation, in a coherent and lucid manner.

## II. Methods

**A. Brief Summary of VBDFT(s).** The basis of VBDFT(s) was described before[3] and a summary follows. This is a semiempirical VB method that scales the final energy to a corresponding density functional energy utilizing the DFT energy of the spin-alternate determinant[28,29] and a parameter, $\lambda$, which is the interaction term that couples an electron pair into a bond. For ethylene, $\lambda$ is a positive quantity standing for

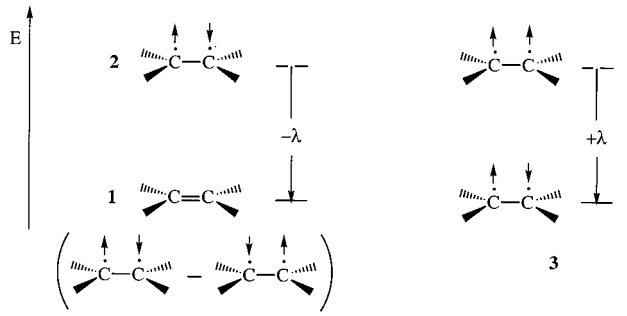


the energy difference between the $\pi$-bonded molecule (**1**) and its spin-alternate determinant (**2**) which possesses two unpaired $p_\pi$ electrons in an antiferromagnetic arrangement, one spin up and one spin down. Thus, $\lambda$ accounts for the energy lowering due to the spin pairing energy of two electrons to a bond pair. In fact, in this picture $\lambda$ is also the matrix element that mixes the two spin-alternate determinants into a singlet paired $\pi$-bond. Ionic structures are not included explicitly, and their effect is embedded within the $\lambda$ parameter.[32b−35]

Once the DFT energy for the spin-alternate determinant ($E_{sa}$) is calculated[3,36] and the value of $\lambda$ is also obtained, one can calculate the energy of all the other relevant determinants and either diagonalize the VB determinant basis set or construct from it a set of Rumer structures that correspond to chemical structures, and then proceed to diagonalize the Rumer basis set.[3] Because the Rumer basis set involves *chemically meaningful structures*, we have chosen to focus on this option and to utilize the "spin-free" approach[37−41] to generate states (see equations in Appendix 2).

The number of Rumer structures rises steeply with the number of electrons, and therefore truncation of the Rumer basis is necessary. The size consistency of the truncation[28c] was tested by comparing the full and truncated results for $C_{14}H_{16}-C_{20}H_{22}$. The level of truncation that gave good results is discussed later in the Results section.

**B. Parametrization of $\lambda$.** In the original application,[3] $\lambda$ was determined using ethylene. Subsequently, it was found that using butadiene which is a more typical "polyene" gives a somewhat better numerical performance for a larger data set, presumably because the $\lambda$ values incorporate effectively long-range orbital distortion.[33] The present paper uses the latter $\lambda$ values. For the $1^1A_g$ ground state of butadiene, the spin-free method[37−41] shows that the energy is lowered relative to the spin-alternate determinant by $\sqrt{3}\lambda$ (see later, Scheme 5b). Therefore, for the ground state $\lambda_g$ is determined from DFT calculations using eq 1.

$$\lambda_g = \frac{\sqrt{3}}{3}[E_{sa} - E(1^1A_g)] \tag{1}$$

By changing the uniform bond length $r$ of butadiene, one finds $\lambda_g$ as a function of the bond length as in eq 2.

$$\lambda_g = 0.6850 - 0.6722r + 0.1720r^2 \tag{2}$$

where $\lambda_g$ is in a.u. and $r$ in Å.

Similarly, from the spin-free method, the excitation energy $1^1A_g \rightarrow 2^1A_g$ for butadiene is $2\sqrt{3}\lambda$ (see Scheme 5). Therefore, to get spectroscopic $\lambda$ values, we carried out CASPT3 and MRCI calculations (using the MOLPRO package[42]) of the excitation energy for a uniform bond length butadiene, and we obtained the value of $\lambda_s$ from eq 3.

$$\lambda_s = \frac{\sqrt{3}}{6}[E(2^1A_g) - E(1^1A_g)] \tag{3}$$

By varying $r$, the expression for $\lambda_s$ becomes eq 4.

$$\lambda_s = 0.4435 - 0.4168r + 0.1021r^2 \tag{4}$$

Thus, VBDFT(s) is a two-parameter method: one parameter describes the ground state and the other the excitation gap, analogous to the treatment of Malrieu et al.[28] All excitation energies were calculated using $\lambda_s$ values only.

Optimized geometries for ground state all-trans polyenes from $C_4H_6$ to $C_{28}H_{30}$ were carried out in $C_{2h}$ symmetry, using B3LYP/6-31G calculations, as implemented in Gaussian 94.[43] The resulting C−C bond lengths show that bond alternation persists all the way to the longest polyene, in line with known data.[21,22] The C−C bond lengths are collected in the table in Appendix 1. Our VBDFT(s) program is still not equipped with an automatic geometry optimization procedure, so optimized excited-state geometries, when used, were taken from literature.[12] In a few cases, geometries were optimized by VBDFT(s) in a pointwise manner by varying the only C−C distances along the bond-alternating mode.

## III. Qualitative VB Theory for Polyenes

Appendix 2 provides the spin-free equations[37−41] for the Rumer-based method, while this section develops the qualitative guides to use the VB theory and thereby understand the

**SCHEME 1: (a) Spectrum of the Rumer Basis Set for *n*-Electron Pairs. (b) Schematic Representation of the Elementary Excitation of the Electron Pairs, and Energy Terms for a Paired Bond and a Couple of Nonbonded Electrons (c) Spin Alternant Determinant (spins shown by arrows)**

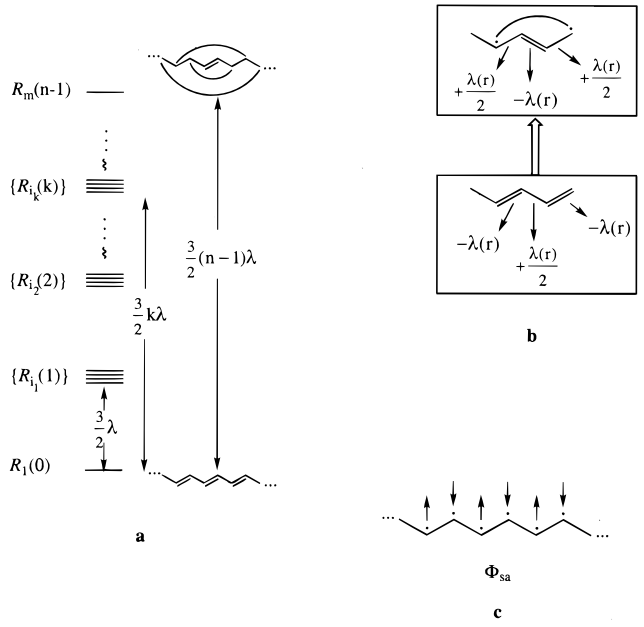


variations of energy gap between the different Rumers, their overlaps, matrix elements, and their mixing patterns.

**Description of the Rumer Basis.** For singlet states, diagonalization of the Rumer basis set will lead to a spectrum of covalent singlet states of $A_g$ and $B_u$ symmetry. Our focus here is on the ground state and the two lowest excited states. The total number of Rumer basis structures for $C_{2n}H_{2n+2}$ polyenes is given by eq 5 (based on eq (A.2.4) in Appendix 2).

$$d_{\text{full}} = \binom{2n}{n} - \binom{2n}{n-1} \tag{5}$$

The structures are described in Scheme 1. The lowest energy structure, is the fundamental Rumer which involves $n$ short $\pi$-bonds. The uppermost Rumer possesses a single $\pi$-bond in the center of the molecule, while the rest of the electrons are paired into $n-1$ long bonds which do not contribute to the VB energy in our scheme. Thus, the uppermost Rumer is $(n-1)$ tuplet excited relative to the fundamental Rumer, and is indicated as $R_m(n-1)$. The rest of the Rumers fall into blocks which differ in their excitation rank, relative to the fundamental structure, and involve successive excitations of short bonds into long ones till $R_m(n-1)$ is reached (see **a** in Scheme 1). A Rumer belonging to a general block is indicated by $R_i(k)$ where $k$ is the excitation rank, and is simply the number of long bonds possessed by all the Rumers of the $k$ block.

The $\pi$-energy associated with a Rumer structure can be written based on eq (A.2.3) of the spin-free theory. A helpful mnemonic is drawing **b** in Scheme 1 which indicates that each pair of bonded electrons lowers the $\pi$-energy by an amount $-\lambda$, while a pair of nonbonded electrons raises the energy by $+0.5\lambda$. The destabilizing nonbonded interaction has been explained[28] to arise from the fact that the wave function of two nonbonded electrons contains 50% triplet relationship between the two electrons, hence resulting in a repulsive interaction which is half as much as the bonding interaction. Drawing **b** shows also that *the elementary excitation energy*, short-bond → long-bond, involves a net loss of one $-\lambda$ for the broken short bond and the creation of a new nonbonded repulsion, $+0.5\lambda$. For a uniform geometry, the elementary excitation energy is given by

$$\Delta E(\text{short bond} \rightarrow \text{long bond}) = \frac{3}{2}\lambda \tag{6}$$

and this is also the spacing between the different blocks in Scheme 1a. The energy of a block $k$ relative to the fundamental Rumer is then simply $k$-fold the elementary excitation energy, as indicated also in Scheme 1a.

The energy of a Rumer structure involves a balance of the short $\pi$-bonds and close neighbor nonbonded interactions. Relative to the spin-alternate determinant (**c** in Scheme 1, with energy $E_{sa}$), this energy is given by

$$E(R_i) = E_{sa} - \sum_{i_b} \lambda(r_{i_b}) + \frac{1}{2}\sum_{i_{nb}} \lambda(r_{i_{nb}}) \tag{7}$$

where the first summation is over the short $\pi$-bonds while the second summation is over the close neighbor nonbonded interactions.

For example, in an alternated geometry which conserves the $C_{2h}$ point group symmetry, the energy of the fundamental Rumer will be given by eq 8

$$E(R_1) = E_{sa} - n\lambda(r_b) + \frac{(n-1)}{2}\lambda(r_{nb}) \tag{8}$$

where $r_b$ is the distance across the short $\pi$-bonds and $r_{nb}$ is the nonbonded close neighbor distance. All other expressions can be written using the above simple recipe.

As shown later, the most important excited Rumer blocks for understanding the ground and the first covalent excited states are the singly and doubly excited ones. The singly excited block involves one long bond, and its configurations are indicated by $R_i(1)$. The number of configurations in this block, $d_1$ is given by eq 9.

$$d_1 = \binom{n}{2} \tag{9}$$

These configurations can be classified into two categories according to their transformation properties with respect to the symmetry operations of the $C_{2h}$ point group.[30] The first category involves *unique structures* that transform as the totally symmetric representation $A_g$. An important structure among the unique ones is the Kekulé structure $R_K$ that possesses $n-1$ short bonds and a long one across $C_1-C_{2n}$. In the second category are the structures which possess a long bond off-center, and therefore each such Rumer has a *twin-structure*. These twins transform to each other by the 2-fold rotation and center of inversion symmetry operations. Scheme 2 illustrates these key features of the singly excited block structures, $R_i(1)$, for $n = 4$. The numbering of the configurations corresponds to their energy ordering in the bond alternated geometry of the ground state. Shown are two unique structures which transform as the totally symmetric representation; the Kekulé structure $R_K$ which possesses three short bonds and a long bond across $C_1-C_8$, and $R_2(1)$ in which the long bond stretches across $C_3-C_6$. In addition, there exist two pairs of twins which are mutually transformable via the operations of the inversion $i$ and the 2-fold rotation $C_2$ operators. As a result, their positive combinations transforms as $A_g$ while their negative combinations transform as $B_u$.

**SCHEME 2: Singly Excited Rumer Structures for $C_8H_{10}$ and Their Symmetry Properties**

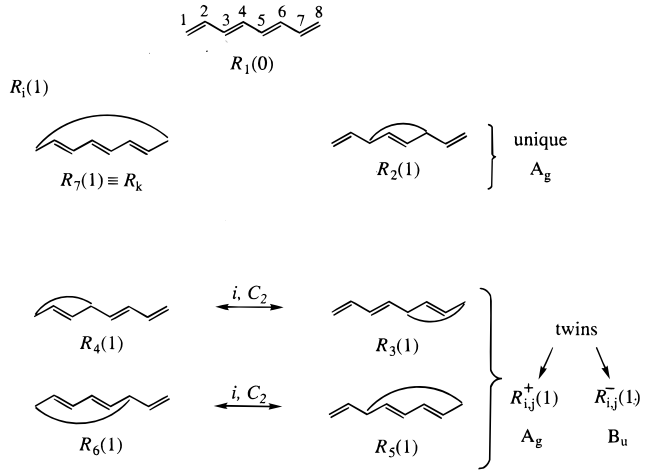


**SCHEME 3: Doubly Excited Rumer Structures for $C_8H_{10}$ and Their Symmetry Properties**

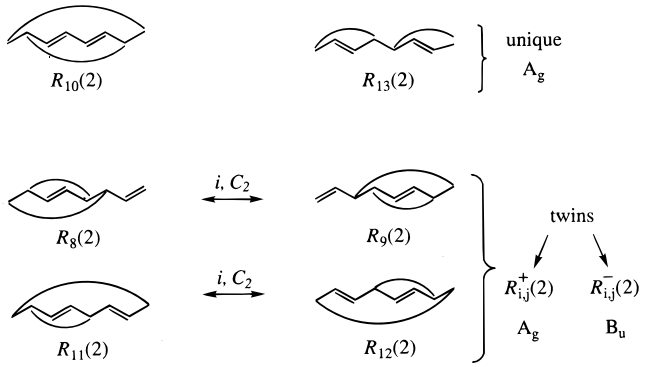


The doubly excited block, $R_i(2)$, includes all of the structures that possess two long bonds. The number of structures in this block are given by eq 10,

$$d_2 = 2\binom{n}{4} + \binom{n}{3} \tag{10}$$

and their main features are based on the same principles as discussed for the singly excited block. Scheme 3 shows the unique and twin structures for $C_8H_{10}$. It is seen that the unique structures arise when the two long bonds both stretch, albeit with different bites, over the central part of the polyene, and when they are distributed symmetrically over the molecular center. The logic behind the twin structures is also quite obvious and as described before they will form positive combinations which transform as $A_g$ and negative combinations which transform as $B_u$.

The number of structures in the triply excited Rumer block is given by eq 11. The structures of this block have a minor effect on the excitation energy (see later) but are required to eliminate size-inconsistency due to truncation.

$$d_3 = 5\binom{n}{6} + 5\binom{n}{5} + \binom{n}{4} \tag{11}$$

**Overlap of Rumer Structures.** A simple mnemonic follows that *translates the spin-free theoretical equations in Appendix 2 to pictorial cartoons.*

Let us start with the overlap property which is independent of geometry and is due to the fact that Rumer structures involve common VB determinants based on $p_\pi$ AOs.[1,3] Based on eq A.2.2 in Appendix 2, the overlap of two Rumers can be written as follows:

**SCHEME 4: Pictorial Method for Determining Overlap of Rumer Structures: (a) Overlap of the Rumers of $C_4H_6$ (b) Definition of an "Elementary Shift" Which Transform One Rumer into Another, and the Corresponding Overlap. (c−e) Examples of "Shifts" and Corresponding Overlaps. (f) Disallowed "shift" that Creates Crossing Bonds**

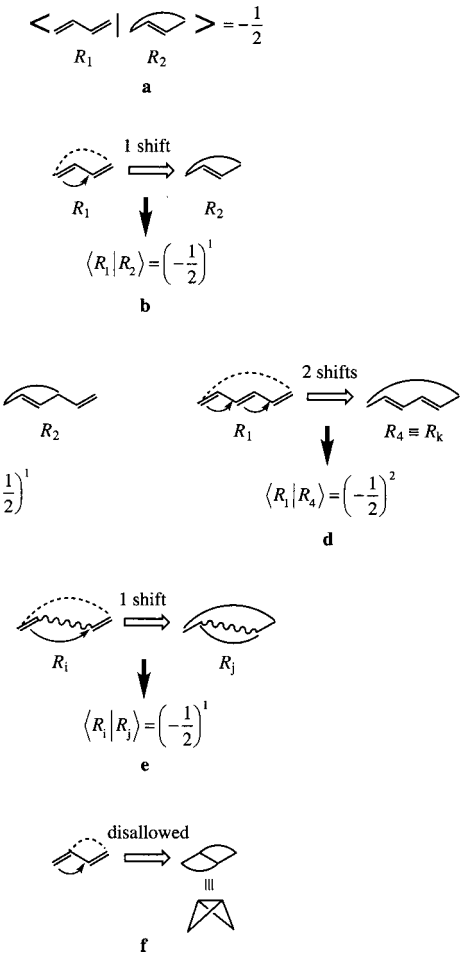


$$\langle R_i | R_j \rangle = \left(-\frac{1}{2}\right)^s \tag{12}$$

where the exponent $s$ is the number of "steps" required to convert one Rumer into the other by means of pairwise transposition of electron indexes. Consider the calculated overlap between the $R_1$ and $R_2$ structures of butadiene in in Scheme 4 (a). This overlap is $-1/2$, since it can be shown that it is possible to interconvert the structures by a single index transposition. Namely, a single step is required to convert $R_1$ to $R_2$ and vice versa. Using this overlap as a starting point, we can represent the overlap of any two arbitrary Rumers by shifting the electron pairing from a paired position to a nonbonded position, in a manner similar to the way organic chemists shift electron pairs, albeit with some differences.

Let us define the "elementary shift" that is shown in Scheme 4(b) for the same two Rumer structures of butadiene in (a). The elementary shift is composed of shifting the $\pi$-pairing into the nonbonded space of a single bond. Once this is done, the other two electrons will be paired automatically across the 1−4

**SCHEME 5: (a) Rumer Structures, Energies, and Reduced Matrix Element for $C_4H_6$. (b) Corresponding Rumer Mixing Diagram Showing the Generation of $1^1A_g$ and $2^1A_g$ from Rumer Structures**

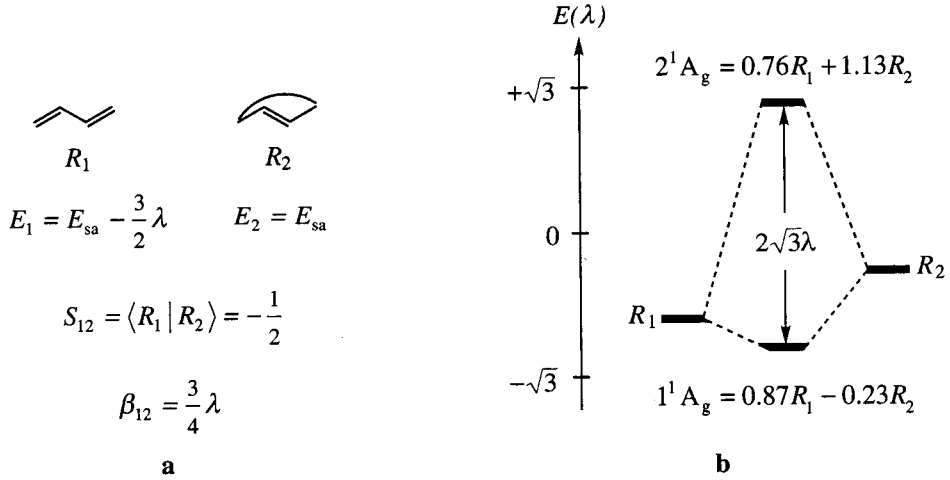


linkages, as shown by the dashes connecting terminal atoms. Thus, the elementary shift applied on $R_1$ is the generator of $R_2$. For this elementary shift, the overlap of the Rumers will be defined according to eq 14 as $-(1/2)$. Thus, the overlap between two Rumers will equal $-(1/2)^s$, where $s$ is the number of elementary shifts required to interconvert the Rumer structures.

There are two types of elementary shifts: short-range and long-range ones. Short-range shifts are shown in (c) and (d) for $C_6H_8$. In (c), one elementary shift generates $R_2$ from $R_1$, and in (d) two elementary shifts are needed to generate $R_4$ from $R_1$. A long-range shift is illustrated in (e), and is seen to have a similar result to the short-range one; the $\pi$-pairing moves to the space between the two bonds, while the termini of the two bonds get automatically paired (indicated by the dashed curve in (e)). Any shift which forms crossing bonds, e.g., shifting the pairing across an odd-number of carbons, as in (f), is disallowed.[44]

It is convenient to start with the fundamental Rumer, from which all the singly excited Rumers are generated by a systematic application of short-range shifts, while the doubly excited Rumers require combinations of short- and long-range shifts, and so on until one generates the entire Rumer basis.[45] The $\langle R_i|R_j\rangle$ overlaps follow eq 12, where $s$ is the number of minimal shifts required to obtain $R_j$ from $R_i$, or vice versa.

An important overlap to consider is between the fundamental Rumer and its Kekulé counterpart. For the general case of $C_{2n}H_{2n+2}$, we need $(n-1)$ elementary short-range shifts to generate $R_K$ from $R_1$, and therefore the overlap will be given by eq 13.

$$\langle R_1|R_K\rangle = \left(-\frac{1}{2}\right)^{n-1} \tag{13}$$

This overlap will gradually diminish with size, and at an infinite chain the two structures have a zero overlap, as has already been pointed out by Klein et al.[29]

**Matrix Elements between Rumer Structures.** The meaningful matrix elements in VB theory are the reduced matrix elements[1,46] given by

$$\beta_{ij} = H_{ij} - eS_{ij} \tag{14}$$

where $e = \min(e_i,e_j)$ and/or $e = (e_i + e_j)/2$; $H_{ij}$ is the unreduced matrix element, $\langle R_i|H|R_j\rangle$; $S_{ij}$ is the corresponding overlap; and $e_i$ is the self-energy of $R_i$.

Scheme 5 shows these quantities for butadiene in a uniform geometry. In (a) it is seen that the reduced matrix element (for $e = e_1$) is given by $(3/4)\lambda$ where $\lambda$ is the interaction term for a short $\pi$-bond. Since the overlap is negatively signed and $\lambda$ is a positive quantity, the ground state will be made from the negative combination of the two Rumers as shown in (b), while the excited state will correspond to the positive combination. In fact, the signs of the linear combinations in the ground and excited state can be deduced from the sign of the overlap of the Rumers using a simple rule: Whenever the overlap of two Rumers is negatively signed, the lower state will be the negative linear combination, while the upper state will be the positive combination. A positively signed overlap, on the other hand, leads to a lower state which is the positive linear combination and an upper state which is the negative combination.

Due to the dependence of the reduced matrix elements on three variables, our qualitative wisdom concerning the general behavior of these matrix elements is still limited. We found that it was possible to reduce the Hamiltonian and obtain reasonable behaviors for the $1^1A_g$ and $2^1A_g$ states, either by using in eq 14; $e = e_1$ uniformly or the averaging formula $e = (e_i + e_j)/2$. From these attempts we can make the following generalizations limited to open-chain polyenes $C_{2n}H_{2n+2}$:

(i) The reduced matrix element between $R_1$ and any excited Rumer $R_i(j)$ is given by

$$\beta_{1i} = -\frac{3}{2}\lambda S_{1i} s_{sr} = -\frac{3}{2}\lambda\left(-\frac{1}{2}\right)^s s_{sr} \tag{15}$$

where $S_{1i}$ is the overlap between $R_1$ and $R_i(j)$ and $s$ is the total number of elementary shifts required to obtain $R_i(j)$ from $R_1$ (including short- and long-range shifts), while $s_{sr}$ is the number of short-range elementary shifts. The reasoning for that is rooted in the fact that the $\lambda$ value is nonzero only for neighboring atoms.[3] Consequently, long-range shifts will contribute zero to the reduced matrix element. Since $\lambda$ is positive, the reduced matrix element, $\beta_{1i}$, and the corresponding overlap, $S_{1i}$, are oppositely signed, leading to a bonding combination which is signed as the sign of the overlap between the respective Rumers, $R_1$ and $R_i(j)$.

(ii) Qualitatively speaking, for a general case the less similar the Rumers, the smaller will be their reduced matrix element.

## IV. Results

**The Effect of Truncating the Rumer Basis.** The VB energies have been calculated for $C_{2n}H_{2n+2}$ species up to $n =$

**TABLE 1: Effect of Truncation of the Rumer Space on the $1^1A_g \rightarrow 2^1A_g$ Vertical Excitation Energy (eV) for $C_{2n}H_{2n+2}$ ($n = 7-14$)[a]**

| n | # Rumer structures | type | $\Delta E_v(1^1A_g \rightarrow 2^1A_g)$ |
|---|---|---|---|
| 7 | 126 | VB(S,D) | 2.95 |
| | 175 | VB(S,D,T) | 2.93 |
| | 429 | VB(full) | 2.93 |
| | 429 | VB(full) | 2.93[b] |
| 8 | 224 | VB(S,D) | 2.74 |
| | 714 | VB(S,D,T) | 2.70 |
| | 1430 | VB(full) | 2.70 |
| | 1430 | VB(full) | 2.70[b] |
| 9 | 373 | VB(S,D) | 2.57[c] |
| | 1549 | VB(S,D,T) | 2.51 |
| | 4862 | VB(full) | 2.51 |
| | 4862 | VB(full) | 2.51[b] |
| 10 | 540 | VB(S,D) | 2.47 |
| | 2520 | VB(S,D,T) | 2.36 |
| | 16796 | VB(full) | 2.36 |
| | 16796 | VB(full) | 2.36[b] |
| 11 | 890 | VB(S,D) | 2.40 |
| | 5831 | VB(S,D,T) | 2.25 |
| | 58786 | VB(full) | 2.23[b] |
| 12 | 1276 | VB(S,D) | 2.36 |
| | 10351 | VB(S,D,T) | 2.16 |
| | 208012 | VB(full) | 2.17[b] |
| 13 | 1794 | VB(S,D) | 2.35 |
| | 742900 | VB(full) | 2.12[b] |
| 14 | 2457 | VB(S,D) | 2.34 |
| | 2674440 | VB(full) | 2.09[b] |

[a] B3LYP geometry is used − see Appendix 1. [b] Evaluated from the error expression for VB(S,D): error(eV) = $0.284 - 0.295e^{-d(S,D)/1106}$; $d(S,D) = d_1 + d_2$ (see eqs 9 and 10). An error expression as a function of the number of truncated Rumers gives smaller errors. [c] $\Delta E$=3.46 eV with VB(S).

14. At present the program efficiency is limited by a rather slow diagonalization routine, and truncation of the basis is required for the large systems. Truncation is classified in hierarchy of excitations. Thus, VB(S) corresponds to inclusion of only singly excited Rumers in addition to the fundamental, while VB(S,D) includes also doubly excited ones, etc.

Table 1 shows the effect of truncating the Rumer basis on the $1^1A_g-2^1A_g$ excitation energy for $C_{14}H_{20}-C_{24}H_{26}$. Use of only singly excited Rumer structures is insufficient. Truncation beyond triply excited Rumers gives quantitatively the same results as the full Rumer set for the cases where the full Rumer set could still be computed, $C_{14}H_{20}-C_{20}H_{22}$. Importantly, truncation of all structures beyond double excitation produce excitation energies which are within 0.02−0.15 eV of results from the full Rumer set. Using an error function enables to estimate the results for the full Rumer set from the VB(S,D) calculations. One can see that VB(S,D,T) is quantitatively excellent, while the maximum error of the VB(S,D) level is ca. 0.285 eV. Thus, there is no significant effect of size inconsistency on the excitation energy, and the trends in the excitation energies can be analyzed using the singly and doubly excited Rumer blocks only.

**VB Excitation Energies.** Table 2 shows the VB vertical excitation energies alongside available experimental data[47−49] and values calculated by sophisticated ab initio methods such as CASPT2[11,12] and multireference Möller−Plessett perturbation (MRMP)[14] treatments. The VB results are seen to be in remarkably good agreement with data available from reliable sources.

Table 3 shows a good match of the VB values of the vertical excitation , vertical emission, and adiabatic excitation energies for $C_8H_{10}$ to the corresponding values calculated by CASPT2 and obtained from experiment.[12] Entries 4 and 5 show the same type of values for $C_4H_6$, and the match is again good.

**TABLE 2: Vertical Excitation Energies (eV) $\Delta E(1^1A_g \rightarrow 2^1A_g)$, for All trans $C_{2n}H_{2n+2}$ Polyenes[a]**

| | $\Delta E_v(1^1A_g \rightarrow 2^1A_g)$, eV | | | |
|---|---|---|---|---|
| n | CASPT2[b] | MRMP[c] | VBDFT(s)[d] | exptl |
| 2 | 6.27 | 6.31 | 6.29 | |
| 3 | 5.19 | 5.09 | 5.02 | 5.21[e] |
| 4 | 4.38 | 4.47 | 4.19 (4.45)[f] | 4.41[g] |
| 5 | | 3.65 | 3.63 | 3.48[h] |
| 6 | | | 3.23 | >2.68[i] |
| 7 | | | 2.93 | >2.34[i](2.93) |
| 8 | | | 2.70 | >2.22 (2.72) |
| 9 | | | 2.51 | |
| 10 | | | 2.36 | |
| 11 | | | 2.25 | |
| 12 | | | 2.16 | |
| 13 | | | 2.12 | |
| 14 | | | 2.09 | |
| ∞ | | | 1.95 ± 0.1[j] | |

[a] The ground-state geometries are specified in Table A1. [b] References 11 and 12. [c] Reference 14. [d] This work. The values for $n = 13, 14$ are estimated from the error function (Table 1). [e] Cited in ref 11. [f] The value in parentheses was obtained by use of the CASSCF geometry in ref 12. [g] References 12 and 47. [h] Reference 48. [i] Adiabatic values from ref 49. In parentheses are estimated vertical values. [j] This value is an average of the following values: The fit for $n = 2-12$ (Figure 1) yields 2.05 eV. Fitting only the results for $n = 7-11$ gives a value of 1.83 eV (exponential fit) or 1.86 eV (polynomial fit). Using the maximum error (error expression in Table 1) yields 1.98 eV. We note that the $VB(S,D)_\infty$ value is 2.266 eV.

**TABLE 3: Vertical and Adiabatic ($1^1A_g \rightarrow 2^1A_g$) Excitation and Emission Energies (eV) for $C_8H_{10}$ and $C_4H_6$**

| | $\Delta E_v$(excitation) | $\Delta E_{00}$ | $\Delta E_v$(emission) |
|---|---|---|---|
| $C_8H_{10}$ | | | |
| CASPT2[a] | 4.38 | 3.61 | 2.95 |
| VBDFT(s)[b] | 4.45[c](4.19) | 3.52[c] | 2.84[c] |
| exptl | ≤4.41 | 3.59 | 3.1 |
| $C_4H_6$ | | | |
| CASPT2 (exptl) | 6.27 | (5.40[d]) | |
| VBDFT(s) | 6.29 | 5.54 | 4.93 |

[a] From ref 12. [b] This work. [c] The values out of parentheses are obtained with the CASSCF geometries in ref 12. The parenthetical value is obtained for the B3LYP geometry in Table A1 of this paper. [d] From ref 6.

The $1^1B_u^-$ state has been shown by Tavan and Schulten[17] to lie for long polyenes just above the "hidden" state $2^1A_g$ and to lead to the weakly allowed $1^1A_g \rightarrow 1^1B_u^-$ transition. A recent theoretical study by Li and Paldus[30] shows that this state has a mixed covalent and ionic character, and therefore it was deemed interesting to compare the results of our VB calculations with those derived by Nakayama et al.[14] using MRMP theory, and with the conclusions of Tavan and Schulten.[17] Table 4 shows the VBDFT(s) and MRMP excitation energies, and while the VB values are consistently lower, the match of the two sets is reasonably good. The last column in the table shows the $2^1A_g-1^1B_u^-$ energy differences which indicates that the two states should approach one another as the polyene gets longer. Their energy gaps seem to decrease, albeit slowly near 0.5 eV. We are therefore in full agreement with the prediction of Tavan and Schulten[17] about the presence of the $1^1B_u^-$ state alongside and very near the hidden state.

Figure 1 shows the $1^1A_g \rightarrow 2^1A_g$ vertical excitation values (Table 2), obtained with the VB method, plotted against number of carbons in the polyene chain. The plot shows the experimentally observed[5,16] falloff of the excitation energy as the chain

**TABLE 4: VBDFT(s) Vertical Excitation Energies to the $1^1B_u^-$ State, and Energy Gaps between the $2^1A_g$ and $1^1B_u^-$ States for $C_{2n}H_{2n+2}$ Polyenes.**

| n | MRMP[a] | $\Delta E(1^1A_g \rightarrow 1^1B_u^-)$[b] | $\Delta E(2^1A_g \rightarrow 1^1B_u^-)$[b] |
|---|---|---|---|
| 3 | 6.31 | 6.22 | 1.20 |
| 4 | 5.76 | 5.34 | 1.15 |
| 5 | 4.91 | 4.68 | 1.05 |
| 6 | | 4.16 | 0.93 |
| 7 | | 3.76 | 0.83 |
| 8 | | 3.44 | 0.74 |
| 9 | | 3.29 | 0.72 |
| 10 | | 3.14 | 0.67 |
| 11 | | 3.02 | 0.62 |
| 12 | | 2.94 | 0.58 |
| 13 | | 2.89 | 0.54 |
| 14 | | 2.84 | 0.50 |

[a] From ref 14. [b] Starting with $n = 9$ onward, VB(S,D) was used.

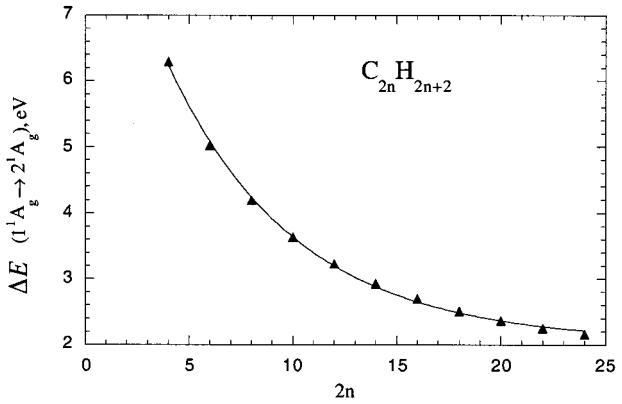


**Figure 1.** Dependence of the $1^1A_g \rightarrow 2^1A_g$ vertical excitation energy on the polyene length for $C_{2n}H_{2n+2}$.

gets longer. The exponential fit leads to eqs 16a and 16b

$$\Delta E(1^1A_g \rightarrow 2^1A_g) \quad \text{eV} = 2.05 + 8.0022\ e^{-0.1617(2n)} \quad n = 2 - 12 \tag{16a}$$

$$\Delta E(1^1A_g \rightarrow 2^1A_g) \quad \text{eV} = 1.83 + 5.99346\ e^{-0.12(2n)} \quad n = 7-12 \tag{16b}$$

Equation 16a, which fits all of the data set, gives an intercept value of 2.05 eV at $n \rightarrow \infty$ (0.22 eV lower than VB(S,D)). Using the error function to evaluate the intercept from the VB(S,D) data gives a consistent value of 1.98 eV. Equation 16b fits only the data for the higher polyenes, where the excitation energy changes very slowly in the range of 2.95−2.16 eV and gives and intercept value of 1.83 eV. A polynomial fit to the same data of eq 16b gives virtually the same result, an intercept value of 1.86 eV. This suggests that at an infinitely long chain, the excitation energy should converge to a finite value of 1.95 ± 0.1 eV. The adiabatic excitation energy in *trans*-polyacetylene is 1.97 eV for the $1^1B_u^+$ state.[6,28b] From this value, an adiabatic excitation of ca. 1−1.4 eV can be estimated for $2^1A_g$, and hence the projected corresponding vertical value (which for finite polyenes is ca. 0.5−0.8 eV higher than the adiabatic one) is in reasonable accord with the above converged value of 1.95 ± 0.1 eV. We note that the VBDFT(s) vertical excitation energies at uniform geometries also converge to a finite value, thus showing that the two states are separated by some intrinsic finite quantity which was called by Schulten and Tavan[17] the covalent gap and which merits understanding in terms of our Rumer structures.

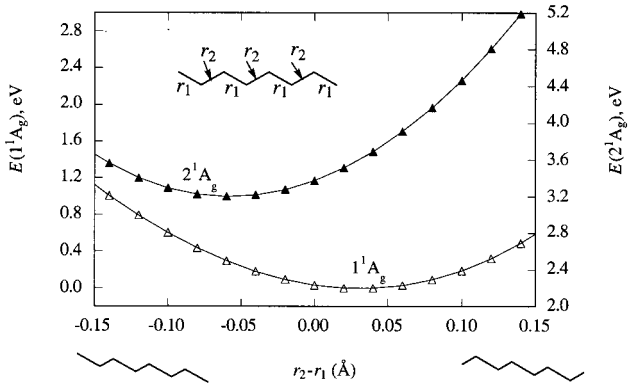


**Figure 2.** Energy variation of the $1^1A_g$ and $2^1A_g$ states of $C_8H_{10}$ along the $a_g$ coordinate. The $1^1A_g$ energy scale is read on the left-hand side while for $2^1A_g$ on the right-hand side.

Figure 2 shows the potential energy curves of the $1^1A_g$ ground state and the $2^1A_g$ excited state for $C_8H_{10}$ plotted along the totally symmetric $a_g$ coordinate, given by the bond length difference $r_2 - r_1$, and which inverts the direction of bond length alternation passing through the uniform geometry ($r_1 = r_2 = 1.41$ Å). The minimum of the ground state is obtained at $r_1 < r_2$, while the minimum for the excited state is located at $r_1 > r_2$ (1.44 Å and 1.38 Å). This is in accord with sophisticated calculations by Roos et al.[12] and Nakayama et al.[14] who showed that the bond alternation for the $2^1A_g$ state is opposite that in the $1^1A_g$ ground state. The same conclusion is deduced from experimental study of substituent effects on the excitation energy and on the vibrational modes, for polyenes up to $C_{16}H_{18}$.[49] Semiempirical calculations[6] reveal that the $2^1A_g$ state undergoes reversal of the bond alternation in the central section $C_3-C_{2n-2}$ of the polyene, whereas the terminal bonds remain short as in the $1^1A_g$ state. For $C_{10}H_{12}$, the semiempirical prediction is not corroborated by the MRMP[14] datum which reveals a bond alternated structure for $2^1A_g$. There are no ab inito data for longer polyenes to be compared with semiempirical predictions for $2^1A_g$ state geometries. Our own method is not equipped with an automatic geometry optimizer to tackle the precise geometric details. But, be the situation as it may, it is clear that as the polyene grows, its $2^1A_g$ state will exhibit reversed bond alternation, at least in a significant section of the polyene.

Comparison of the energy rise of the two curves in Figure 2 (read left vs right-hand scales) from their respective minimum shows that the excited-state potential is steeper than the ground-state potential. The same trend is obtained for other polyenes, which we have tested ($C_{2n}H_{2n+2}$; $n = 2-5$). The relative steepness of the states would require an exalted frequency of the $a_g$ C═C stretching mode for the excited state, in line with experimental observations[5,6,49] and ab initio calculations.[50]

**VB Wave Functions.** The number of the Rumer structures becomes quite large as the polyene grows (Table 1). However, a few features of the wave function can still be understood with reference to two key structures, which are the fundamental structure $R_1$ and its Kekulé pair $R_K$ (see, e.g., Scheme 2). Table 5 shows the coefficients and weights of these Rumer structures for the ground state and $2^1A_g$ excited state of a few polyenes. Each entry involves subentries, which correspond respectively to the situations in the ground-state geometry (a), in a uniform bond length geometry (b), and in the excited-state geometry (c). Inspection of the data in Table 5 shows that at the ground-state geometry, the fundamental Rumer structure has the highest weight in $1^1A_g$, while $R_K$ makes a minor contribution that decreases as the polyene gets longer.

**TABLE 5: VBDFT(s) Coefficients (*c*) and Weights (*w*) of the Fundamental Rumer Structure ($R_1$) and Its Kekulé Partner, ($R_K$) for $C_{2n}H_{2n+2}$ Polyenes in the Ground and Excited States**

| | | $1^1A_g$ | | | $2^1A_g$ | | |
|---|---|---|---|---|---|---|---|
| entry[a] | n | $c_1, w_1$ | $c_K, w_K$ | $w$(S)[b] | $c_1, w_1$ | $c_K, w_K$ | $w$(S,D)[c] |
| 1a | 2 | 0.87, 0.85 | −0.23, 0.15 | 0.15 | 0.76, 0.15 | 1.13, 0.85 | 0.85 |
| 2a | 3 | 0.73, 0.70 | 0.09, 0.04 | 0.29 | 0.75, 0.19 | −0.72, 0.61 | 0.81 |
| 2b | 3 | 0.65, 0.60 | 0.15, 0.08 | 0.39 | 0.73, 0.24 | −0.79, 0.64 | 0.76 |
| 2c | 3 | 0.53, 0.46 | 0.24, 0.15 | 0.51 | 0.72, 0.30 | −0.85, 0.63 | 0.70 |
| 3a | 4 | 0.61, 0.56 | −0.04, 0.01 | 0.39 | 0.64, 0.18 | 0.40, 0.32 | 0.81 |
| 3b | 4 | 0.50, 0.44 | −0.08, 0.04 | 0.49 | 0.58, 0.20 | 0.50, 0.40 | 0.79 |
| 3c | 4 | 0.42, 0.34 | −0.13, 0.07 | 0.57 | 0.54, 0.22 | 0.57, 0.44 | 0.77 |
| 4a | 5 | 0.50, 0.45 | 0.02, 0.01 | 0.46 | 0.53, 0.15 | −0.22, 0.16 | 0.83 |
| 4b | 5 | 0.39, 0.32 | 0.05, 0.02 | 0.53 | 0.44, 0.16 | −0.32, 0.24 | 0.82 |
| 4c | 5 | 0.23, 0.16 | 0.14, 0.08 | 0.62 | 0.36, 0.18 | −0.44, 0.30 | 0.81 |
| (4d)[d] | 5 | | | | 0.43, 0.18 | −0.33, 0.23 [0.04][d] | |

[a] All entries marked (a) use ground-state geometry, (see Appendix 1). All entries marked (b) use uniform geometry, ($\lambda_s = 0.07$). All entries marked (c) use excited-state geometry. For $n = 4$, the excited-state geometry is taken from ref 12. For $n = 3$, 5, $r_1 = 1.46$ Å and $r_2 = 1.36$ Å are used. [b] $w$(S) includes all $R_i(1)$. [c] $w$(S,D) includes all $R_i(1)$, $R_i(2)$. [d] Data corresponding to semiempirical geometry in ref 6. The value in brackets is the weight of the Rumer structure with short terminal bonds and a long bond stretching over carbons 3 and 8.

The weight of $R_K$ is significant in the $2^1A_g$ excited state and becomes increasingly more important at the uniform geometry and still more so at the excited-state geometry with reversal of bond alternation. For example, in $C_{10}H_{12}$ ($n = 5$), the weight of $R_K$ doubles as the geometry varies from that of the ground state to that of the excited state (compare entries 4c and 4a). In fact, for all polyenes tested, $R_K$ is the dominant excited-state structure at a geometry which exhibits reversed bond alternation relative to the ground state. Note, however, that the other singly and doubly excited Rumers make together a significant contribution to the excited state, as may be seen from the column entitled $w$(S, D).

The last line in the table shows the weight of the structures at the semiempirically predicted geometry[6] of the excited state for $C_{10}H_{12}$, with short terminal bonds and reversed bond alternation in the $C_3-C_8$ section. It is seen that $R_K$ has the highest weight even in this geometry, while the Rumer structure with the long bond stretching over $C_3-C_8$ has a small weight (datum in square brackets). Clearly, the $R_K$ Rumer will be important for the excited state in any geometry that involves reversed bond alternation in a significant portion of the polyene. As the polyene grows, $R_K$ and other Rumers which possess long bonds extending over a major portion of the polyene, e.g., $C_3-C_{2n-2}$, $C_1-C_{2n-2}$, and $C_3-C_{2n}$, will all become important and lead to a geometry with reversed bond alternation over a significant length of the polyene.

An interesting feature in Table 5 is the relative sign of mixing of $R_1$ and $R_K$, which is precisely as in the corresponding antiaromatic/aromatic cyclic species,[1,51−53] and may be understood based on the sign alternation of the overlap (and hence also of the reduced matrix element) between $R_1$ and $R_K$ which is given by $(-1/2)^{n-1}$ in eq 12.

## Discussion

Understanding the behavior of the Rumer structures and their mixing patterns provides some insight into the nature of the ground state and its covalent singlet excited states. To illustrate the insight we use $C_6H_8$ and analyze it in excruciating detail, which will assist us later to generalize the conclusions to higher polyenes. There exist five covalent structures which are shown in drawings **4**−**8**.

Figure 3 shows Rumer mixing diagrams for $C_6H_8$. Part (a) constructs from the twin-pairs of the singly excited structures ($R_2$, $R_3$) the positive and negative linear combinations which transform as $A_g$ and $B_u$, respectively. Subsequently, in part (b),

**4** $R_1$

**5, 6** $R_2, R_3$

**7** $R_4 \equiv R_k$

**8** $R_5$

we mix all of the Rumers according to their symmetry properties. Thus, the $R^-_{2,3}$ combination that transforms as $B_u$ finds no symmetry match and forms the $1^1B_u^-$ state. The four $A_g$ combinations form in turn four $A_g$ states, $1^1A_g - 4^1A_g$, but we show in Figure 3(b) only the first two corresponding to the ground state and the hidden excited state.

The ground state $1^1A_g$ is nascent from $R_1$, which mixes all other Rumers in bonding combinations (oppositely signed to the corresponding overlaps). The mixing of the doubly excited Rumer ($R_5$) is quite small, and hence its contribution is not shown explicitly. The hidden excited state, $2^1A_g$, is nascent from $R_K$ which mixes in a sandwich fashion with $R_1$, $R^+_{2,3}$, and $R_5$.

To understand this sandwich interaction better, we show it gradually in parts (c) and (d). Thus, in diagram (c), we mix $R_1$ initially with $R^+_{2,3}$ to form $\Phi_1$ and $\Phi_1{}^*$. Subsequently, in part (d) these two Rumer combinations, as well as $R_5$, mix with $R_K$ from above and below to form the $2^1A_g$ state that ends up involving $R_1$ and $R^+_{2,3}$ with the same sign of mixing (note that this is an antibonding relationship of the two). Thus, the final energy of $2^1A_g$ will be set by the balance of the sandwich interaction of $R_K$.

Figure 4 shows a Rumer correlation diagram for $C_6H_8$ along the bond-alternation coordinate which transforms as the totally symmetric representation and is hence the $a_g$ mode coordinate. A few trends can be pointed out.

The fundamental Rumer is stabilized at $r_2 - r_1 > 0$ and is destabilized in the opposite direction of the coordinate. This behavior of $R_1$ is in accord with its tendency to maximize the stabilizing $\pi$-bonding energy along the short bonds which are along the C−C linkages having $r_1$ distances, and its tendency to minimize the repulsive nonbonded interactions which are

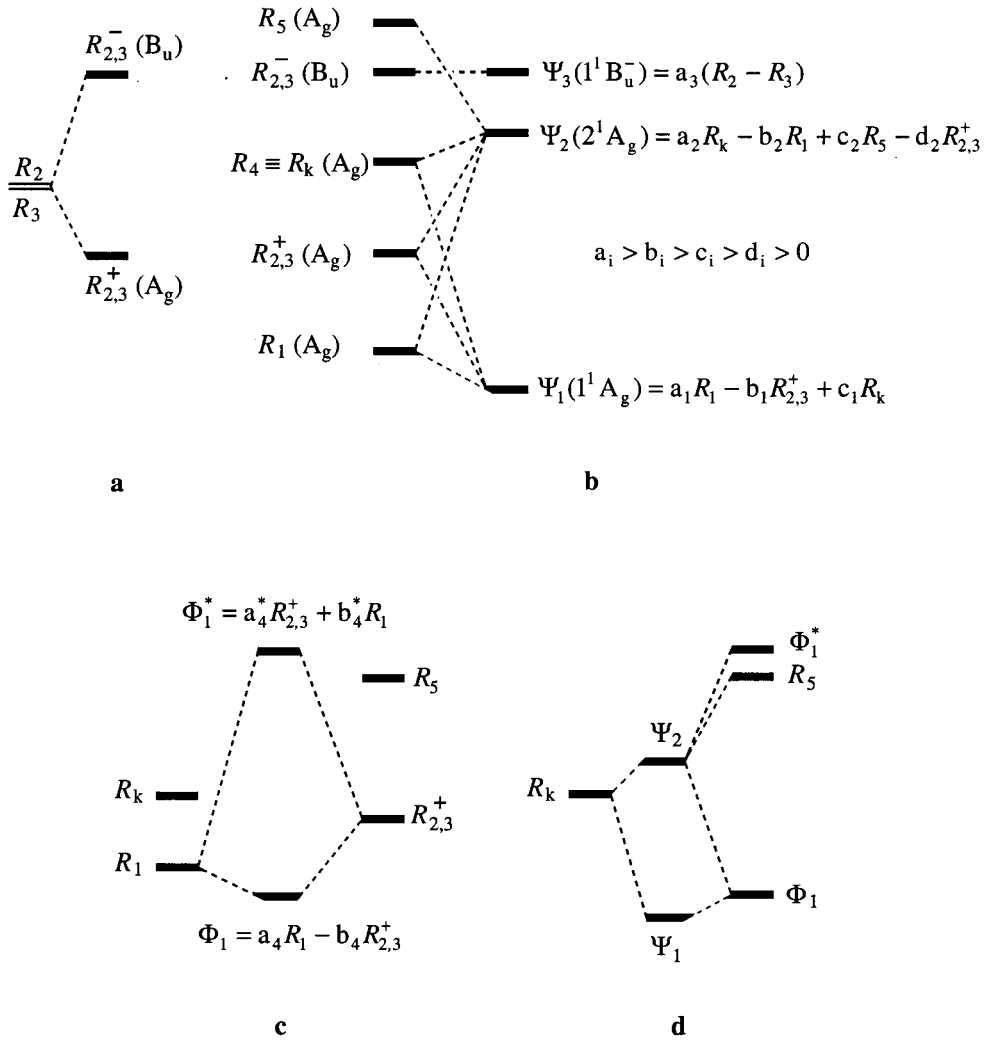


**Figure 3.** Rumer mixing diagram for $C_6H_8$. (a) Construction of the symmetry adapted combinations of $R_2$ and $R_3$. (b) Mixing of the symmetry matched structures and the resulting states. (c, d) Stepwise Rumer mixing diagrams which illustrate the bonding−antibonding interactions embedded in the $2^1A_g$ state.

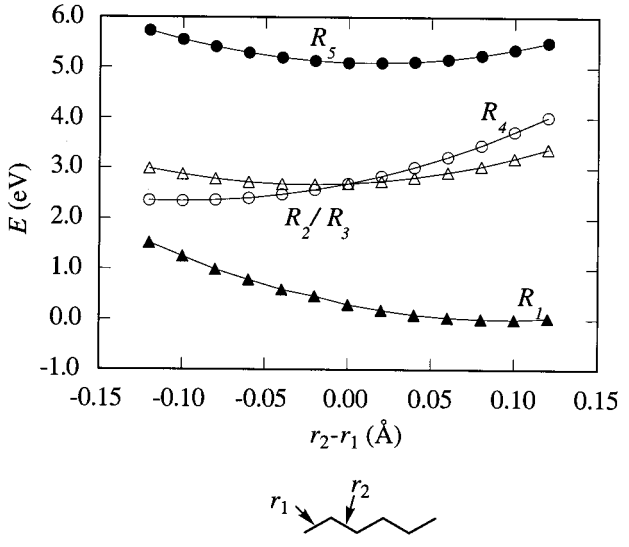


**Figure 4.** A Rumer correlation diagram along the $a_g$ (bond alternation) coordinate.

across the linkages having an $r_2$ distance. The ground-state minimum of $C_6H_8$ is located at $r_2 - r_1 > 0$, near the minimum of the $R_1$ curve.

The Rumers of the singly excited block, $R_2 - R_4$, are degenerate at the uniform geometry ($r_2 - r_1 = 0$) but spread into a two-below-one or to a one-below-two on the two sides of the uniform geometry. The Kekulé structure $R_K$ ($R_4$) has a minimum at a geometry corresponding to $r_2 - r_1 < 0$. This is in accord with the fact that now the short $\pi$-bonds are across the C−C linkages which possess $r_2$ distances. In fact, the minimum of the hidden excited state, $2^1A_g$, is near the minimum of the Kekulé structure $R_K$. It follows therefore that both the ground state, $1^1A_g$, and the hidden excited state, $2^1A_g$, prefer a bond-alternated structure but will exhibit opposite bond alternation patterns. We further note that among the singly excited Rumers, $R_K$ experiences the strongest relaxation along the $a_g$ coordinate, simply because it contains the maximal number of short $\pi$-pairs which are stabilized along this coordinate, while at the same time the nonbonded repulsive $\pi$-interactions along the single bonds can be minimized along the same coordinate.

**General Trends in $C_{2n}H_{2n+2}$.** The basic features of Figures 3 and 4 are quite general, albeit more Rumer structures join the key players as the polyene grows longer. Thus, the ground state, $1^1A_g$, will be nascent from $R_1$ mixed in primarily with all of the positive combinations of the twin-pair singly excited Rumers, $R_{i,j}^+(1)$. The $R_{i,j}^+(1)$ pairs that mix the most with $R_1$ are those which differ from $R_1$ by the smallest number of elementary shifts, and hence will possess a long bond with the shortest

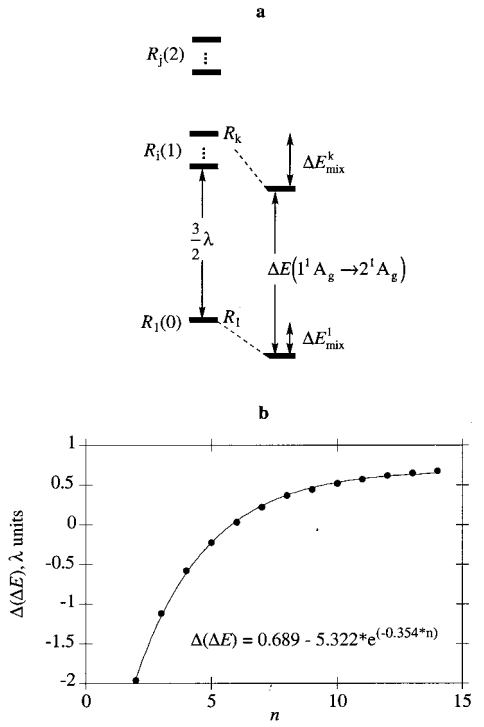


**Figure 5.** (a) The relation of the excitation energy, $\Delta E(1^1A_g \rightarrow 2^1A_g)$, to the original $R_1-R_K$ energy gaps, and the mixing energy quantities of these configurations. (b) The convergence of the difference mixing energy quantities of $R_1$ and $R_K$ (eq 17) as a function of the polyene length.

possible range. Smaller contributions arise from $R_K$ and other unique $R_i(1)$ structures. Still smaller (and negligible) contributions will come from doubly excited structures.

The $1^1B_u^-$ state will generally be the third covalent state, $\Psi_3$, and will be constructed from all the negative combinations, $R_{ij}^-(1)$, of the twin-pairs in the singly excited block, mixed with eachother in a bonding fashion, with smaller contributions coming from the analogous twin combinations of the doubly excited blocks, $R_{i,j}^-(2)$.

The hidden excited state will involve $R_K$ mixed in an antibonding manner with $R_1$ and in a bonding manner with all other unique structures that are singly and doubly excited, as well as with all positive combinations of twin-pairs, $R_{i,j}^+(1)$ and $R_{i,j}^+(2)$, which belong to the singly and doubly excited blocks (the $R_1$ and the $R_{i,j}^+(1)$ pairs will maintain an antibonding relation between them). Since the long bond of $R_K$ stretches over the termini of the polyene, $R_K$ will mix more strongly with those Rumer structures that possess long bonds with the longest possible bite (this ensures the largest overlap and reduced matrix element). It follows, therefore, that the $2^1A_g$ state will involve Rumers having contiguous double−single bond alternation in long sections of the polyene, e.g., $C_1-C_{2n-2}$, $C_3-C_{2n}$, and $C_3-C_{2n-2}$. Thus, even though the state involves an extensive mixture of Rumer structures, it will bear $R_K-$ likeness.

We may therefore regard $R_1$ and $R_K$ as the generators of $1^1A_g$ and $2^1A_g$, and focus hereafter on the behavior of these two Rumers, to understand trends in the $1^1A_g - 2^1A_g$ states.

**Convergence of the Excitation Gap for Large Polyenes.** Let us proceed first to understand the pattern of the $1^1A_g-2^1A_g$ vertical excitation energy, as observed in experiment[5,6,16,49] and as presented by the VB results in Figure 1. Figure 5(a) shows a schematic diagram that depicts the emanation of the $1^1A_g$ and $2^1A_g$ states from the generator Rumer structures. For simplicity, we consider here the case of a uniform geometry. Thus, initially $R_1$ and $R_K$ are separated by $(3/2)\lambda$ which is the elementary excitation energy involved in going from the fundamental Rumer to the singly excited block (recall Scheme 1a). By allowing the Rumer structures to mix with eachother, the $R_1$ structure develops into the ground state and is lowered by $\Delta E^1_{mix}$. Similarly, $R_K$ mixes with the other singly as well as with the doubly excited Rumers, develops into the excited state ($2^1A_g$), and is lowered by $\Delta E^K_{mix}$. The excitation gap can be written then as

$$\Delta E(1^1A_g \rightarrow 2^1A_g) = \frac{3}{2}\lambda - (\Delta E^K_{mix} - \Delta E^1_{mix}) \qquad (17)$$

Initially, for $C_4H_6$ and $C_6H_8$ the $\Delta E^K_{mix}$ quantity is negative due to the overriding antibonding interactions suffered by $R_K$ as described in Figure 3. Starting with $C_8H_{10}$, the mixing quantity becomes negative and stabilizing due to the increasing number of doubly excited Rumer structures. As the polyene continues to grow, the difference of the mixing terms of $R_1$ and $R_K$ will begin to converge to a finite quantity. Figure 5b shows a plot of $\Delta(\Delta E^K_{mix} - \Delta E^1_{mix})$ in units of $\lambda$, against $n$, for a uniform polyene. It is apparent that the difference of the mixing quantities converges to a finite value which is somewhat less than $(3/4)\lambda$. As a result, the excitation energy of the uniform chain converges itself to a value which is very nearly $(3/4)\lambda$, ca. 1.1−1.5 eV, depending on the value of $r$ at the uniform geometry. The same convergence of the mixing quantity is expected, and is in fact observed for a bond alternate polyene whether it is for the vertical excitation or the adiabatic excitation energies (see Figure 1). An upper bound for the excitation energy for the infinite polyene chain can be written as eq 18, by assuming that the $\Delta(\Delta E^K_{mix} - \Delta E^1_{mix})$ quantity converges to zero for a bond alternated structure.

$$\Delta E(1^1A_g \rightarrow 2^1A_g)_{n\rightarrow\infty} \approx \frac{3}{2}\lambda_{av} \qquad (18)$$

Here the quantity $\lambda_{av}$ is the average value (1.4−1.5 eV) which sets the upper bound value of the excitation energy at 2.1−2.3 eV, in the range of the converged vertical value in Figure 1 (eq 16). It is seen then, that the intrinsic gap between the ground state and the hidden excited state of a polyene is simply the elementary excitation of unpairing one short bond to one long bond, as schematically depicted in Scheme 1b.

**Bond Alternation Properties in the Ground and Excited States.** $R_K$ which completely alternates the short and long bonds relative to $R_1$ has the largest potential of stabilization along the bond alternation coordinate. All of the singly excited Rumers share a few short bonds, in the same positions as in the fundamental Rumer, and as such, their potential stabilization by geometric relaxation is limited to the site of the excitation. For long polyenes, the singly excited Rumer structures with long bonds in positions $C_1-C_{2n-2}$, $C_3-C_{2n}$, and $C_3-C_{2n-2}$, etc., share with $R_K$ a significant common length of reversed bond alternation, and as such they will all be stabilized along $a_g$ coordinates which involve a significant bond alternation.

Figure 6 is a generalized Rumer correlation diagram, showing $R_1$ and $R_K$ Rumer structures, along the $a_g$ mode. The first important trend seen in the figure is the opposite sense of bond alternation exhibited by the two Rumers. Using the theoretical section we may write based on eq 8, the expressions for the energy of $R_1$ at the bond-alternated geometry and at the uniform geometry. For a bond-alternated geometry where the $n$ short $\pi$-bonds are across the short $r_1$ distances and are associated with a large $\lambda$ value ($\lambda_l$), while the $n-1$ nonbonded interactions are

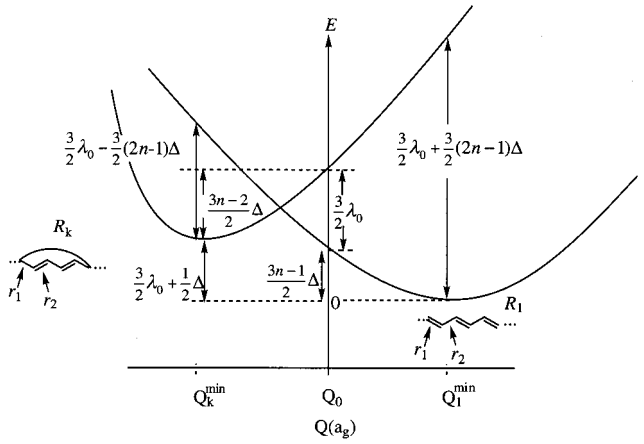


**Figure 6.** A general behavior and energetics of $R_1$ and $R_K$ along the bond alternation coordinate.

across the longer $r_2$ distances and have a small $\lambda$ value ($\lambda_s$), the energy will be given by eq 19.

$$E(R_1)_{alt} = E_{sa} - n\lambda_l + \frac{(n-1)}{2}\lambda_s \qquad (19)$$

For a uniform geometry with $\lambda = \lambda_0$, the energy expression reduces to eq 20.

$$E(R_1)_0 = E_{sa} - \frac{(n+1)}{2}\lambda_0 \qquad (20)$$

Assuming a simple relation between all of these $\lambda$ values,

$$\lambda_l = \lambda_0 + \Delta \qquad \lambda_s = \lambda_0 - \Delta \qquad (21)$$

The energy stabilization of $R_1$ by bond alternation will be given by,

$$E(R_1)_{alt} - E(R_1)_0 = -\frac{(3n-1)}{2}\Delta \qquad (22)$$

In a similar manner for $R_K$, in the bond-alternated geometry, where now $r_1$ is longer than $r_2$, there exist $n-1$ $\pi$-bonds and $n$ nonbonded repulsions across the longer linkages. Accordingly the energy expression is

$$E(R_K)_{alt} = E_{sa} - (n-1)\lambda_l + \frac{n}{2}\lambda_s \qquad (23)$$

At the uniform geometry, this becomes

$$E(R_K)_0 = E_{sa} - \frac{(n-2)}{2}\lambda_0 \qquad (24)$$

Using the expressions for the $\lambda$ in terms of the uniform $\lambda_0$, the stabilization of $R_K$ due to bond alternation follows as

$$E(R_K)_{alt} - E(R_K)_0 = -\frac{(3n-2)}{2}\Delta \qquad (25)$$

Because $R_K$ possesses the maximal number of short bonds among the singly excited Rumers, it will enjoy the largest stabilization by bond alternation and will drive the $2^1A_g$ excited state toward this geometry. Since $\Delta$ is a significant quantity, 0.3−0.4 eV, the bond alternation propensity of $R_1$ and $R_K$ will be very strong and will dominate the behavior of their respective states, which will in turn exhibit bond alternation in opposite senses along the $a_g$ coordinate.[29b] The intrinsic energy of the $\sigma$-frame given by $E_{sa}$, which does not prefer bond alternation, and the effect of mixing of other Rumer structures (e.g., with $C_1-C_{2n-2}$, $C_3-C_{2n}$, and $C_3-C_{2n-2}$, long bonds) will modify the geometries and will introduce fluctuation from perfect bond alternation,[6] but will not disrupt the trends established by $R_1$ and $R_K$. We may therefore, generalize, that for $C_{2n}H_{2n+2}$, the ground and hidden excited states will both exhibit approximate bond alternation in opposing senses. As the polyene grows, this bond alternation reversal, even if not stretching across the full length, will still be maintained in a significant portion of the polyene. Very crudely speaking, the adiabatic $1^1A_g \rightarrow 2^1A_g$ excitation may be described based in Figure 6 as a bond shift attended by concomitant inversion of the bond-length alternation, in a significant length of the polyene.

**The Frequency of the Totally Symmetric C═C Stretching Mode.** To understand the trends in the $\omega(a_g)$ frequency of the C═C mode, consider the mixing patterns of the two key Rumers in the vicinities of their respective minima in Figure 6 (consult also Figure 4 for $C_6H_8$). The energy difference between the fundamental and the excited Rumer structures is larger near $Q_1^{min}$ and decreases toward $Q_K^{min}$. Consequently, $R_1$ enjoys the least stabilization energy by VB mixing near its own minimum $Q_1^{min}$, whereas away from the minimum toward $r_1 > r_2$, the energy gap decreases and the mixing increases. Similarly, to the right of $Q_1^{min}$, the mixing increases since $\lambda$, the mixing parameter, increases. Consequently, the ground-state curve will become shallow around $Q_1^{min}$, leading to a low frequency for the $a_g$ mode.

Understanding the steepness of the excited state is a bit more complex because $2^1A_g$ is obtained from $R_K$ by a balance of bonding and antibonding interactions with the other structures. However, it is clear from Figure 6 that $R_1$ and $R_K$ approach one another near the $Q_K^{min}$ minimum. Eventually the two Rumers will cross one another along the $a_g$ coordinate. From the energy expressions of the two Rumers in the alternate geometry, near $Q_K^{min}$, and by use of the condition for crossing ($E_1 = E_K$), it is possible to derive a general condition for the crossing, in eq 26

$$\Delta = \frac{\lambda_0}{(2n-1)} \qquad (26)$$

This expression provides the means to locate the crossing point for any given $\lambda_0$ value. Using the value for $r_0 = 1.41$ Å, it is possible to find the values of $\Delta$ which will correspond to a crossing point for any given n in $C_{2n}H_{2n+2}$. It is apparent that for short polyenes $n = 2$ and 3 the crossing will require large $\Delta$, corresponding to unrealistic geometries. Thus, for $C_4H_6$ ($n = 2$), our calculated crossing point corresponds to $r_1 = 1.57$ Å and $r_2 = 1.25$ Å, which corresponds almost to a fragmented molecule. As $n$ gets larger $\Delta$ gets closer to zero, which means that the crossing will shift gradually toward the uniform geometry, and the infinitely long polyene will resemble an infinite $C_{2n}H_{2n}$ ring.

The crossing of $R_1$ and $R_K$ was verified also for $C_8H_{10}-C_{12}H_{14}$. In the vicinity of the crossing point, $1^1A_g$ and $2^1A_g$ correspond to bonding and antibonding combinations of $R_1$ and $R_K$ which contribute, in turn, approximately equal weights to the two states. This avoided crossing picture is reminiscent of the Kekulé mixing picture,[52a,53,54] which was used before to account for the exalted frequency of the $b_{2u}$ mode in the $1^1B_{2u}$ excited state of benzene. In the benzene case, the two Kekulé structures intersect along the $b_{2u}$ mode, and by avoided crossing lead to a low $\omega(b_{2u})$ frequency in the ground state and an exalted

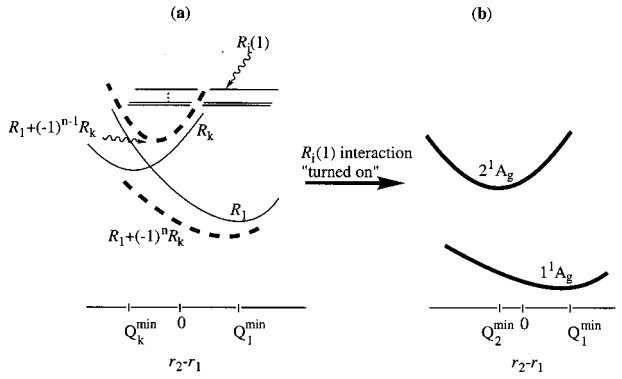


**Figure 7.** (a) Crossing and avoided crossing of $R_1$ and $R_K$ along the bond alternation coordinate. The resulting avoided crossing combinations are traced by dashed-bold lines. (b) The $1^1A_g$ and $2^1A_g$ states after the "turning on" of the interaction with all other singly excited Rumer structures, $R_i(1)$. After this latter mixing, near the corresponding minima of each state, the $1^1A_g$ state is shallower than $R_1$, while the $2^1A_g$ retains the memory of the avoided crossing and is steeper than $R_K$. Note that in the $1^1A_g$ ground state, the C═C mode motion follows the bonding properties of $R_1$, while in the $2^1A_g$ excited state the motion follows the $\pi$-bond reversal inherent in the $R_1-R_K$ avoided crossing.

one in the $1^1B_{2u}$ excited state. In the present problem, the situation is more complex because the $R_1-R_K$ crossing occurs at a geometry where all other singly exited Rumers are close in energy and mix into the two states. To decipher the problem, we studied the $C_8H_{10}$ and $C_{10}H_{12}$ cases in details and the results are depicted in Figure 7.

Thus, Figure 7a shows the avoided crossing (by dashed-bold curves) of $R_1$ and $R_K$ along the bond alternation coordinate. As a result of the avoided crossing, one forms a lower combination which is shallower than $R_1$, and a higher combination flanked between the rising branches of both $R_1$ and $R_K$, and hence is much steeper than either Rumer structure in the avoided crossing region. Above the upper combination there lie all other singly excited Rumer structures, labeled as $R_i(1)$. In a second step, in Figure 7b, we turn on the interaction of these $R_i(1)$ structures which, by mixing with the $R_1 \pm R_K$ combinations, generate the final $1^1A_g$ and $2^1A_g$ states. Hence, due to the increased mixing of $R_1$ with higher lying singly excited Rumers, the $1^1A_g$ potential becomes shallow along the $a_g$ mode, as the ground-state geometry varies to-and-fro around $Q_1^{min}$. The excited state, on the other hand, retains the memory of the $R_1/R_K$ avoided crossing, and has therefore a steeper potential around $Q_2^{min}$. This steeper potential is the root cause of the exalted $\omega(a_g)$ frequency in $2^1A_g$. Thus, even though there is a significant blending of a sea of Rumer structures in each state, in the end the $\omega_{C=C}(1^1A_g)$ frequency reflects the behavior of $R_1$ and its mixing patterns as the C−C bonds swing back and forth about their equilibrium values in $Q_1^{min}$. In contrast, the exalted $\omega_{C=C}(2^1A_g)$ frequency reflects the behavior of an antibonding avoided crossing state combination of $R_1$ and $R_K$. Thus, the exalted C═C frequency in the $2^1A_g$ excited state of polyenes is reminiscent of the behavior of the Kekulé mode ($b_{2u}$) in benzene and other acenes.[52a,53,54]

In fact, the $R_1/R_K$ avoided crossing model for the excited state frequency can account for an additional trend, namely that the upshift of the C═C frequency generally gets larger as the polyene chain gets longer.[49] Thus, it is apparent from Figures 6 and 7a that, as the polyene grows longer and the crossing point shifts toward the uniform geometry (eq 26), the two crossing curves become steeper in the crossing region since their

**SCHEME 6: Behavior of the Excited State Resulting from the Avoided Crossing of $R_1$ and $R_K$, for $C_{2n}H2_{n+2}$, along the Bond Alternation Coordinate (a) for Larger $n$ Values, when the Crossing Takes Place near $Q_K^{min}$, and (b) when the Crossing Takes Place near the Uniform Geometry**

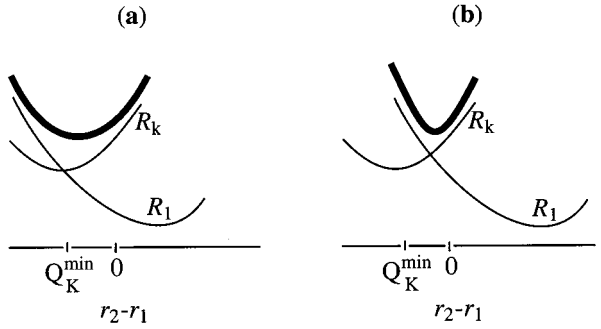


energies relative to the curve minima increase in proportion to $n$ (see eqs 22 and 25). Consequently, due to avoided crossing, the antibonding combination will become gradually steeper, leading eventually to an increase of the C═C frequency in $2^1A_g$ (as shown in a vs b in Scheme 6). One can further predict that the frequency of the excited state should ultimately converge because the number of excited Rumers that mix into the avoided crossing state (Figure 7b) increases, thus mitigating the steepness of the state as the polyene grows longer.

The role of the $R_K$ structure in the increase frequency of the $\omega_{C=C}$ mode has been deduced before by Kohler et al.[49] who ascribed the frequency exaltation to the "double bond reversal" relative to the ground state. Kohler has concluded that the bond-alternation reversal inherent in the VB picture accounts better than other models for several observations regarding the hidden excited state (e.g., the frequency exaltation, the signs of anharmonicity in the ground and excites states, and the stability patterns of the excited state). Kamisuki et al.[55a] have used an empirical VB treatment similar to that of Scherer et al.,[55b] to account for the upshift of the C═C frequency in $C_8H_{10}$.

**Possible Other Manifestations of the Valence Bond Picture.** The $R_1/R_K$ crossing can have an important impact on the connection of the ground and excited states. Thus, at the avoided crossing geometry, the $1^1A_g-2^1A_g$ gap is small (e.g., for $C_{10}H_{12}$ the gap is 2.1 eV compared with 3.6 eV at the ground-state minimum). Because the reduced matrix element $\beta_{1K}$ approaches zero as $n$ goes to infinity (eq 15), we expect the avoided-crossing interaction to diminish with the polyene size. This small gap, which is near the $2^1A_g$ minimum, will affect the efficiency of radiationless decay from $2^1A_g$ to $1^1A_g$. Thus, by twisting out of planarity, the mixing parameter $\lambda$ further decreases and the avoided crossing becomes a real crossing and can serve as a funnel from the excited state to the ground state.[56] This has been shown in a series of important papers by Olivucci, Bernardi, and Robb for excited states of a few short polyenes.[57]

$C_8H_{10}$ has been studied extensively by Kohler[5] and by Christensen et al.[47f] and was found to exhibit a low fluorescence quantum yield which increased with terminal substitution, and to undergo very facile isomerization from the trans,trans isomer to the cis,trans and cis,cis isomers. The isomerization mechanism has been elucidated by computational means,[57c] and the fastest process appears to be associated with a conical intersection between $2^1A_g$ and $1^1A_g$, while a slower one involves initial isomerization on $2^1A_g$ followed by decay. Here we merely wish to show the useful insight gained by use of Rumer structures.

Scheme 7 shows two singly excited structures for $C_8H_{10}$. These structures appear also above in Scheme 2, and here we

**SCHEME 7: Singly Excited Rumer Structures with the Long Bonds Depicted as Diradicaloids, and Mechanistic Significance**

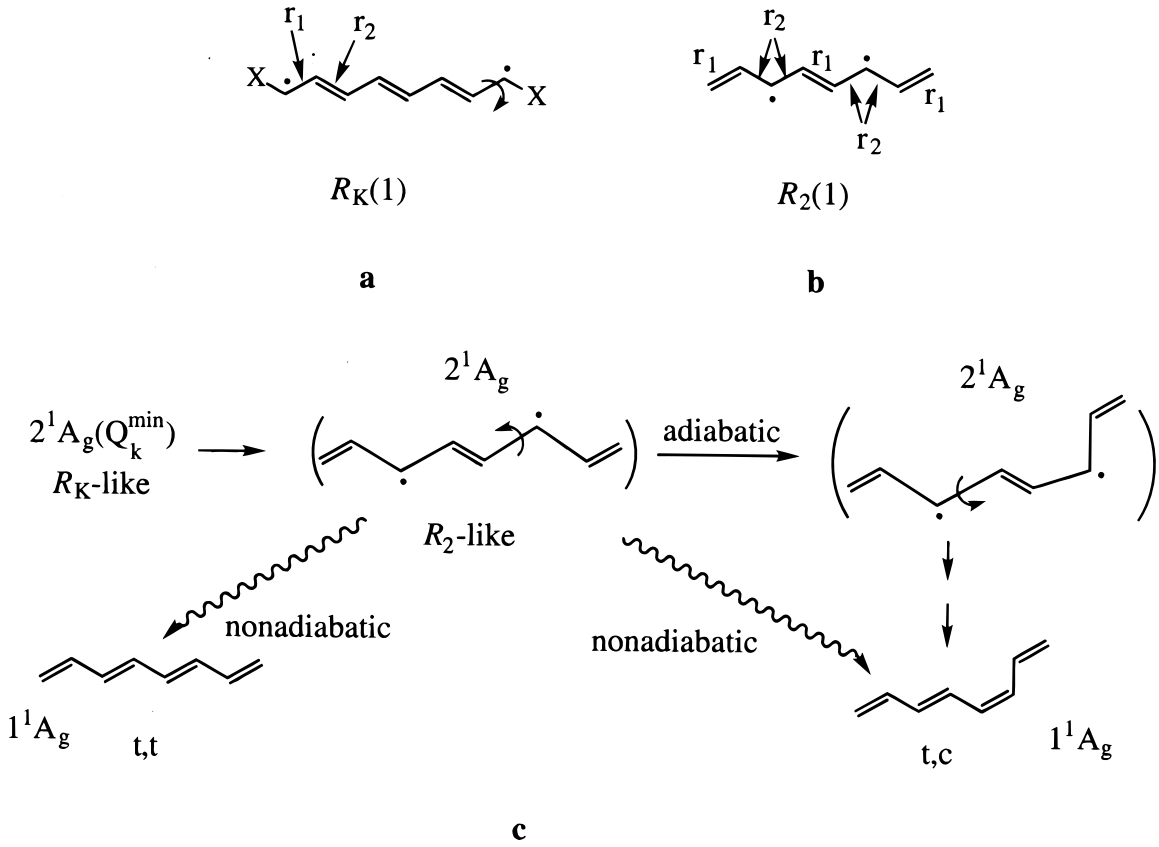


**TABLE A. 1: C−C Bond Lengths of $C_{2n}H_{2n+2}$ Polyenes[a,b]**

| n | $r_1$ | $r_2$ | $r_3$ | $r_4$ | $r_5$ | $r_6$ | $r_7$ | $r_8$ | $r_9$ | $r_{10}$ | $r_{11}$ | $r_{12}$ | $r_{13}$ | $r_{14}$ |
|---|---|---|---|---|---|---|---|---|---|---|---|---|---|---|
| 2 | 1.3554 | 1.4672 | | | | | | | | | | | | |
| 3 | 1.3579 | 1.4592 | 1.3653 | | | | | | | | | | | |
| 4 | 1.3588 | 1.4571 | 1.3685 | 1.4499 | | | | | | | | | | |
| 5 | 1.3592 | 1.4562 | 1.3698 | 1.4470 | 1.3720 | | | | | | | | | |
| 6 | 1.3595 | 1.4558 | 1.3705 | 1.4458 | 1.3737 | 1.4439 | | | | | | | | |
| 7 | 1.3596 | 1.4555 | 1.3709 | 1.4451 | 1.3745 | 1.4423 | 1.3754 | | | | | | | |
| 8 | 1.3597 | 1.4554 | 1.3711 | 1.4447 | 1.3750 | 1.4415 | 1.3765 | 1.4407 | | | | | | |
| 9 | 1.3598 | 1.4552 | 1.3713 | 1.4444 | 1.3754 | 1.4408 | 1.3772 | 1.4394 | 1.3777 | | | | | |
| 10 | 1.3597 | 1.4551 | 1.3713 | 1.4442 | 1.3756 | 1.4405 | 1.3775 | 1.4389 | 1.3782 | 1.4385 | | | | |
| 11 | 1.3599 | 1.4551 | 1.3715 | 1.4441 | 1.3757 | 1.4404 | 1.3777 | 1.4386 | 1.3787 | 1.4379 | 1.3790 | | | |
| 12 | 1.3599 | 1.4551 | 1.3715 | 1.4441 | 1.3758 | 1.4403 | 1.3779 | 1.4385 | 1.3789 | 1.4376 | 1.3793 | 1.4373 | | |
| 13 | 1.3599 | 1.4551 | 1.3715 | 1.4441 | 1.3758 | 1.4403 | 1.3779 | 1.4384 | 1.3790 | 1.4374 | 1.3796 | 1.4370 | 1.797 | |
| 14 | 1.3599 | 1.4551 | 1.3715 | 1.4441 | 1.3758 | 1.4403 | 1.3779 | 1.4384 | 1.3791 | 1.4374 | 1.3797 | 1.4369 | 1.3800 | 1.4365 |

[a] Optimized at the B3LYP/6-31G level. [b] Unique bond lengths are reported and are specified in order where the terminal bond is denoted as $r_1$, etc.

draw them in the essential chemical character where the "long-bond" is replaced by a diradical structure. Thus, the Kekulé structure, $R_K$, in a is a 1,8-diradical, and a rotation about its terminal C−C bond will possess a small barrier in comparison with the corresponding process in the ground state. Upon rotation (a more complex motion is shown in ref 57c), the $1^1A_g-2^1A_g$ surfaces will touch and the radiationless conversion from the excited state to the ground state will be facilitated. Terminal substituent X (e.g., Ph), which hinders the rotation, will reduce the radiationless efficiency and increase the fluorescence yield. A similar rationale was given by Kohler et al.[49] for the stability of polyenes conferred by $\alpha,\omega$ substituents such as Ph which stabilize radical centers.

From a broader perspective, the $2^1A_g$ excited state is a mixture of excited Rumer structures where the diradicaloid moiety is distributed in different locations of the polyene. At different geometries, the excited state will have a different dominant character. For example, in the bond alternated geometry where $r_1 > r_2$, $R_K$ will be the dominant character and the diradical will occupy the 1,8 terminals, as in a. In a nonalternated geometry, where two long bonds separate two shorter bonds, the excited state will possess a major $R_2$ character as shown in b, with a diradical in the 3,6 positions. From these different goemetries the polyene excited state can experience different decay and isomerization pathways. In c we show how a geometric distortion which localizes the odd electrons in two $(CH)_3$ units with long C−C bonds, transforms the $2^1A_g$ excited state from $R_K$-like to $R_2$-like. In this geometry the polyene can undergo an adiabatic isomerization on the $2^1A_g$ potential to the trans,cis (t,c) isomer. It has been invincibly demonstrated by Olivucci, Robb, Bernardi, et al.[57c] that the structure of the conical intersection, which leads to radiationless decay, involves a

localized $(CH)_3$ moiety. Thus, the $R_2$-like geometry is also a precursor of a conical intersection, which leads to nonadiabatic isomerization along with decay to the (t,t)-isomer. Finally, it seems reasonable to postulate that different distortions from the bond-alternated $2^1A_g$ minima will generate a variety of shallow local minima which will have characteristics of the different singly excited Rumers. These minima will correspond to bi-solitons which localize singlet paired radicals on different sites of the polyene. As argued above, the more likely positions of the bi-solitons are not too distant from the termini of the polyene (e.g., $C_1-C_{2n-2}$, $C_3-C_{2n}$, and $C_3-C_{2n-2}$, etc bi-soliton). These solitons will be separated from each other by tiny barriers, and therefore one may envision the $2^1A_g$ excited state as a species which performs soliton hopping between quasidegenerate Rumer minima.

## Conclusion

The VBDFT(s) method presented above combines accuracy and simplicity. Its mixing rules enable to gain insight into a variety of properties of the various covalent states of polyene, such as the excitation energies and their convergence at an infinite length of the polyene, the opposite bond alternation of the ground state and the $2^1A_g$ state, and notably the puzzling phenomenon of the C=C frequency exaltation in the $2^1A_g$ state.

**Acknowledgment.** The authors are thankful to Dr. Shi-jun Zhong for preliminary studies. The research in the Hebrew University was supported in part by an internal grant to S.S., and by the VW stiftung and the ISF.

## Appendix 1

The appendix consists of a table (Table A.1) which collects the optimized C−C distances of the polyenes studied in the paper.

## Appendix 2. A Spin-Free Form of VBDFT(s)

The spin-free form of valence bond theory has been discussed using symmetric group approach by McWeeny,[37] Zhang,[38,39] and co-workers. The spin-free form of VBDFT(s) is used in this paper to carry out all calculations using Rumer structures because of its computational and conceptual conveniences. With the approximations used[3] (zero differential overlap between VB determinants, and retention of neighboring $\lambda$ only), the Hamiltonian and overlap matrix elements for linear systems in VBDFT(s) become

$$H_{ij} = E_{sa} S_{ij} - \sum_{k=1}^{N-1} D_{11}^{[\mu]}(P_i^{-1}(k,k+1)P_j)\lambda_{k,k+1} \quad \text{(A2.1)}$$

$$S_{ij} = D_{11}^{[\mu]}(P_i^{-1}P_j) \quad \text{(A2.2)}$$

Here $N$ is the number of electrons of the system, $P_i$ is the permutation acting on electronic indexes by means of a transposition $(k, k+1)$ between indexes $k$ and $k+1$, and thereby transforming Rumer structure $R_1$ to $R_i$. The $D_{11}^{[\mu]}$ term is the first diagonal matrix element of the irreducible representation $[\mu] = [2^{N/2-S}, 1^{2S}]$ for permutation $P$, whereas $S$ is spin multiplicity. The structure $R_1$ is the fundamental structure with a consecutive bonding pattern, $1-2, 3-4, \ldots, (N-1)-N$ (i.e., atom 1 is bonded to 2, 3 to 4, etc.). The value of $D_{11}^{[\mu]}(P)$ has been shown[39−41] to have the form of $(-1)^t(-(1/2))^u$, where $t$ and $u$ depend on the permutation $P$ and the irreducible representation $[\mu]$. For singlet states, $t = 0$. Thus $D_{11}^{[\mu]}(P)$ has a simple form $(-(1/2))^u$. From eq A.2.1 there follows an expression for the energy of Rumer, in eq A.2.3.

$$E(R_i) = E_{sa} - \sum_{k=1}^{N-1} D_{11}^{[\mu]}(P_i^{-1}(k,k+1)P_i)\lambda_{k,k+1} \quad \text{(A.2.3)}$$

A discussions of $u$ is more complex and the interested reader is referred to the original literature.[37−41] In the text we provide qualitative guides for determining this quantity.

The number of Rumer structures is the same as the dimension of the irreducible representation $[\mu]$, and given as eq A.2.4 for any spin situation $S$.

$$m = \binom{N}{\frac{1}{2}N - S} - \binom{N}{\frac{1}{2}N - S - 1} \quad \text{(A.2.4)}$$

## References and Notes

(1) For a recent viewpoint article, see: Hiberty, P. C. *J. Mol. Struct. (THEOCHEM)* **1998**, *451*, 237−261.

(2) (a) See for example the insight gained by applications of the combined VB and molecular mechanics method in Bernardi, F.; Olivucci, M.; Robb, M. A. *J. Am. Chem. Soc.* **1992**, *114*, 1606−1616. Bernardi, F.; Olivucci, M.; Robb, M. A. *Pure Appl. Chem.* **1995**, *67*, 17−24. Garavelli, M.; Celani, P.; Bernardi, F.; Robb, M. A.; Olivucci, M. *J. Am. Chem. Soc.* **1997**, *119*, 6891−6901. (b) For applications of VB ideas to excited states, see for example, Michl, J.; Bonacic-Koutecky, V. *Electronic Aspects of Organic Photochemistry*; Wiley: New York, 1990.

(3) Wu, W.; Zhong, S.-J.; Shaik, S. *Chem. Phys. Lett.* **1998**, *292*, 7−14.

(4) Hudson, B. S.; Kohler, B. E.; Schulten, K. *Excited States*; Lim, E. C., Ed.; Academic Press: New York, 1982; Vol. 6, pp 1−95.

(5) Kohler, B. E. *Chem. Rev.* **1993**, *93*, 41−54.

(6) Orlandi, G.; Zerbetto, F.; Zgierski, M. Z. *Chem. Rev.* **1991**, *91*, 867−891.

(7) Branchadell, V.; Sodupe, M.; Oliva, A.; Bertrán, J. Contribution of Quantum Chemistry to the Study of Dienes and Polyenes, in *The Chemistry of Dienes and Polyenes*; Rappoport, Z., Ed.; John Wiley & Sons: Chichester, 1997; Vol. 1, pp 1−23.

(8) Hudson, B. S.; Kohler, B. E. *Chem. Phys. Lett.* **1972**, *14*, 299−304.

(9) Hudson, B. S.; Kohler, B. E. *J. Chem. Phys.* **1973**, *59*, 4984−5002.

(10) Schulten, K.; Karplus, M. *Chem. Phys. Lett.* **1972**, *14*, 305−309.

(11) Serrano-Andrés, L.; Merchán, M.; Nebot-Gil, I.; Lindh, R.; Roos, B. O. *J. Chem. Phys.* **1993**, *98*, 3151−3160.

(12) Serrano-Andrés, L.; Lindh, R.; Roos, B. O.; Merchán, M. *J. Phys. Chem.* **1993**, *97*, 9360−9368.

(13) Serrano-Andrés, L.; Roos, B. O.; Merchán, M. *Theor. Chim. Acta* **1994**, *87*, 387−402.

(14) Nakayama, K.; Nakano, H.; Hirao, K. *Int. J. Quantum Chem.* **1998**, *66*, 157−175.

(15) Kawashima, Y.; Nakayama, K.; Nakano, H.; Hirao, K. *Chem. Phys. Lett.* **1997**, *267*, 82−90.

(16) Kohler, B. E. *J. Chem. Phys.* **1990**, *93*, 5838−5842.

(17) Tavan, P.; Schulten, K.; *J. Chem. Phys.* **1986**, *85*, 6602−6609.

(18) Schulten, K.; Ohmine, I.; Karplus, M. *J. Chem. Phys.* **1976**, *64*, 4422−4441.

(19) Ohmine, I.; Karplus, M.; Schulten, K. *J. Chem. Phys.* **1978**, *68*, 2298−2318.

(20) Lasaga, A. C.; Aerni, R. J.; Karplus, M. *J. Chem. Phys.* **1980**, *73*, 5230−5243.

(21) Longuet-Higgins, H. C.; Salem, L. *Proc. R. Soc. London* **1959**, *A251*, 172−185.

(22) (a) Fincher, C. R., Jr.; Chen, C.-E.; Heeger, A. J.; MacDiarmid, A. G.; Hastings, J. B. *Phys. Rev. Lett.* **1982**, *48*, 100−104. (b) For a recent theoretical treatment using a variety of methods, see: Choi, C. H.; Kertesz, M.; Karpfen, A. *J. Chem. Phys.* **1997**, *107*, 6712−6721.

(23) See, for example, (a) Krogh-Jespersen, K.; Rava, R. P.; Goodman, L. *J. Phys. Chem.* **1984**, *88*, 5503−5513. (b) Wolf, J.; Hohlneicher, G. *Chem. Phys.* **1994**, *181*, 185−208. (c) Goodman, L.; Berman, J. M.; Ozkabak, A. G. *J. Chem. Phys.* **1989**, *90*, 2544−2554. (d) Wunsch, L.; Metz, F.; Neusser, H. J.; Schlag, E. W. *J. Chem. Phys.* **1977**, *66*, 386-400. (e) Klingensmith, K. A.; Dewey, H. J.; Vogel, E.; Michl, J. *J. Am. Chem. Soc.* **1989**, *111*, 1539.

(24) (a) Su, W. P.; Schrieffer, J. R.; Heeger, A. J. *Phys. Rev. Lett.* **1979**, *42*, 1698−1701. (b) Su, W. P.; Schrieffer, J. R.; Heeger, A. J. *Phys. Rev. B* **1980**, *22*, 2099−2111.

(25) Christensen, R. L.; Kohler, B. E. *J. Chem. Phys.* **1975**, *63*, 1837−1846.

(26) Simonetta, M.; Gianinetti, E.; Vandoni, I *J. Chem. Phys.* **1968**, *48*, 1579−1594.

(27) Dunning, T. H., Jr.; Hosteny, R. P.; Shavitt, I. *J. Am. Chem. Soc.* **1973**, *95*, 5067−5068.

(28) (a) Said, M.; Maynau, D.; Malrieu, J.-P.; Garcia Bach, M.-A. *J. Am. Chem. Soc.* **1984**, *106*, 571−579. (b) Said, M.; Maynau, D.; Malrieu, J.-P. *J. Am. Chem. Soc.* **1984**, *106*, 580−587. (c) Guihery, N.; Ben Amor, N.; Maynau, D.; Malrieu, J.-P. *J. Chem. Phys.* **1996,** *104*, 3701−3708.

(29) (a) Klein, D. J.; García Bach, M.-A. *Phys. Rev. B* **1979**, *19*, 877−886. (b) Klein, D. J.; Schmalz, T. G.; Seitz, W. A.; Hite, G. E. *Int. J. Quantum Chem. Sympos.* **1986**, *19*, 707−718.

(30) Li, X.; Paldus, J. *Int. J. Quantum Chem.* **1999**, *74*, 177−192.

(31) Hirao, K.; Nakano, H.; Nakayama, K.; Dupuis, M. *J. Chem. Phys.* **1996**, *105*, 9227−9239.

(32) (a) Applications to radicals, diradicals, and systems which involve heteroatoms have been recently completed successfully and will be published. Applications to triplet and other states of polyenes have been described in ref 3. (b) In SCVB and GVB theories, ionicity is embedded in the distortion of the atomic orbitals (ref 33, 34). See, however, explicit treatment of ionicity in ref 35.

(33) Cooper, D. L.; Gerratt, J.; Raimondi, M. *Adv. Chem. Phys*; Lawley, K. P., Ed.; John Wiley & Sons: New York, 1987, Vol. 69, pp 319−397.

(34) Goddard, W. A., III.; Harding, L. B. *Annu. Rev. Phys. Chem.* **1978**, *29*, 363−396.

(35) Hiberty, P. C.; Humbel, S.; Byrman, C. P.; van Lenthe, J. H. *J. Chem. Phys.* **1994**, *101*, 5969−5976.

(36) One inputs the spin alternated wave function as a guess into any existing software and obtains the energy of the guess, as described in Hiberty, P. C.; Danovich, D.; Shurki, A.; Shaik, S. *J. Am. Chem. Soc.* **1995**, *117*, 7760−7768.

(37) McWeeny, R. *Int. J. Quantum Chem.* **1988**, *34*, 25−36.

(38) Li, X.; Zhang, Q. *Int. J. Quantum Chem.* **1989**, *36*, 599−632.

(39) Wu, W.; Mo, Y.; Zhang, Q. *J. Mol. Struct. (THEOCHEM)* **1993**, *283*, 227−236.

(40) McWeeny, R. *Methods of Molecular Quantum Mechanics*, 2nd ed.; Academic Press: London, 1992.

(41) Wu, W. Ph.D. thesis, Xiamen University, 1989.

(42) (a) MOLPRO (version 98.1) is a package of ab initio programs written by Werner, H.-J. and Knowles, P. J. with contributions from Almlöf, J.; Amos, R. D.; Berning, A.; Cooper, D. L.; Deegan, M. J. O.; Dobbyn, A. J.; Eckert, F.; Elbert, S. T.; Hampel, C.; Lindh, R.; Lloyd, A. W.; Meyer, W.; Nicklass, A.; Peterson, K.; Pitzer, R.; Stone, A. J.; Taylor, P. R.; Mura, M. E.; Pulay, P.; Schütz, M.; Stoll, H. and Thorsteinsson, T. (b) Multireference perturbation theory (CASPT2/CASPT3), see: Werner, H.-J. *Mol. Phys.* **1996**, *89*, 645−661. (c) Internally contracted MRCI, see: Werner, H.-J.; Knowles, P. J. *J. Chem. Phys.* **1988**, *89*, 5803−5814. Knowles, P. J.; Werner, H.-J. *Chem. Phys. Lett.* **1988**, *145*, 514−522. For excited states see: Knowles, P. J.; Werner, H.-J. *Theor. Chim. Acta* **1992**, *84*, 95−103.

(43) Gaussian 94: Frisch, M. J.; Trucks, G. W.; Schlegel, H. B.; Gill, P. M. W.; Johnson, B. G.; Robb, M. A.; Cheeseman, J. R.; Keith, T.; Petersson, G. A.; Montgomery, J. A.; Raghavachari, K.; Al-Laham, M. A.; Zakrzewski, V. G.; Ortiz, J. V.; Foresman, J. B.; Cioslowski, J.; Stefanov, B. B.; Nanayakkara, A.; Challacombe, M.; Peng, C. Y.; Ayala, P. Y.; Chen, W.; Wong, M. W.; Andres, J. L.; Replogle, E. S.; Gomperts, R.; Martin, R. L.; Fox, D. J.; Binkley, J. S.; Defrees, D. J.; Baker, J.; Stewart, J. P.; Head-Gordon, M.; Gonzalez, C.; Pople, J. A. Gaussian, Inc.: Pittsburgh, PA, 1995.

(44) Crossing bonds create linear dependency of the Rumer basis set. See ref 45.

(45) Pauncz, R. *Spin Eigenfunctions. Construction and Use*; Plenum Press: New York, 1979.

(46) Shaik, S. S. In *New Theoretical Concepts for Understanding Organic Reactions*; Bertrán, J., Csizmadia, I. G., Eds.; Kluwer Academic Publishers: 1989, *C267*, 165.

(47) (a) Heimbrook, L. A.; Kenny, J. E.; Kohler, B. E.; Scott, G. W. *J. Chem. Phys.* **1981**, *75*, 4338−4342. (b) Heimbrook, L. A.; Kohler, B. E.; Levy, I. J. *J. Chem. Phys.* **1984**, *81*, 1592−1597. (c) Leopold, D. G.; Vaida, V.; Granville, M. F. *J. Chem. Phys.* **1984**, *81*, 4210−4217. (d) Allan, M.; Neuhaus, L.; Haselbach, E. *Helv. Chim. Acta* **1984**, *67*, 1776−1782. (e) Bouwman, W. G.; Jones, A. C.; Phillips, D.; Thibodeau, P.; Friel, C.; Christensen, R. L. *J. Phys. Chem.* **1990**, *94*, 7429−7434. (f) Petek, H.; Bell, A. J.; Choi, Y. S.; Yoshihara, K.; Tounge, B. A.; Christensen, R. L. *J. Chem. Phys.* **1993**, *98*, 3777−3794.

(48) D'Amico, K. L.; Manos, C.; Christensen, R. L. *J. Am. Chem. Soc.* **1980**, *102*, 1777−1782.

(49) Kohler, B. E.; Spangler, C.; Westerfield, C. *J. Chem. Phys.* **1988**, *89*, 5422−5428.

(50) Aoyagi, M.; Ohmine, I.; Kohler, B. E. *J. Phys. Chem.* **1990**, *94*, 3922−3926.

(51) Mulder, J. J. C.; Oosterhoff, L. J. *Chem. Commun.* **1970**, *305*, 307.

(52) (a) Shaik, S.; Shurki, A.; Danovich, D.; Hiberty, P. C. *J. Am. Chem. Soc.* **1996**, *118*, 666−671. (b) Shaik, S.; Shurki, A.; Danovich, D.; Hiberty, P. C. *J. Mol. Struct. (THEOCHEM)* **1997**, *398*−*399*, 155−167.

(53) (a) Zilberg, S.; Haas, Y. *Int. J. Quantum Chem.* **1999**, *71*, 133−145. (b) Zilberg, S.; Haas, Y. *J. Phys. Chem. A* **1999**, *103*, 2364−2374.

(54) Shaik, S.; Zilberg, S.; Haas, Y. *Acc. Chem. Res.* **1996**, *29*, 211−218.

(55) (a) Kamisuki, T.; Taya, M.; Maeda, S. *J. Chem. Soc., Faraday Trans.* **1996**, *92*, 3481−3486. (b) Scherer, J. R.; Overand, J. *Spectrochim. Acta*, **1961**, *17*, 719.

(56) For a pioneering recognition of the role of the conical intersection as a funnel in photophysics, see: Gerhartz, W.; Poshusta, R. D.; Michl, J. *J. Am. Chem. Soc.* **1977**, *99*, 4263−4271.

(57) (a) Olivucci, M.; Bernardi, F.; Celani, P.; Regazos, I.; Robb, M. A. *J. Am. Chem. Soc.* **1994**, *116*, 1077−1085. (b) Olivucci, M.; Bernardi, F.; Ottani, S.; Robb, M. A. *J. Am. Chem. Soc.* **1994**, *116*, 2034−2048. (c) Garavelli, M.; Celani, P.; Yamamoto, N.; Bernardi, F.; Robb, M. A.; Olivucci, M. *J. Am. Chem. Soc.* **1996**, *118*, 11656−11657.